TURUN YLIOPISTON JULKAISUJA,
ANNALES UNIVERSITATIS TURKUENSIS

SARJA - SER. A I OSA - TOM. 468

ASTRONOMICA - CHEMICA - PHYSICA - MATHEMATICA

CIRCULAR SPECTRO-POLARIMETRIC STUDIES OF DQ WHITE DWARFS

by

Tommi Vornanen

TURUN YLIOPISTO
UNIVERSITY OF TURKU
Turku 2013

From

Department of Physics and Astronomy
University of Turku
FI-20014 Turku
Finland

Supervised by

Prof. Svetlana Berdyugina
Kiepenheuer Institute Für Sonnenphysik
Wissenschaftsgemeinschaft Gottfried Wilhelm Leibniz
Germany

Reviewed by

Prof. Nikolai Piskunov
Department of Astronomy and Space Physics
Uppsala University
Sweden

Dr. Juhani Huovelin
Department of Physics
University of Helsinki
Finland

Opponent

Dr. Ralf Napiwotzki
Centre for Astrophysics Research
University of Hertfordshire
United Kingdom

ISBN 978-951-29-5494-0 (PRINT)
ISBN 978-951-29-5495-7 (PDF)
ISSN 0082-7002
Painosalama Oy - Turku, Finland 2013

Acknowledgements

I feel that I can not fit everyone I would like to thank on one page so I would like to start by saying that every person I have met in my life has helped me become the person I am today. And since I happen to like myself the way I am, all those people deserve a great big "thank you". That said, there are some people I have to mention by name because they have been a huge influence in my life and/or have helped me finish this thesis.

First, I would like to thank my scientific colleagues. Vilppu Piirola, Andrei Berdyugin and Svetlana Berdyugina have taught me how to do science and thus deserve a big Thank You. While I have been doing this thesis several people have helped me onward on this journey. Thank you Auni Somero, Heidi Lietzen and Sarah Bird for putting up with me at the office, Kari Nilsson for patiently answering my questions and Esko Gardner for programming help and more, Baybars Külebi for scientific discussions. And finally to Esko Valtaoja for supporting me in the final steps. I would also like to thank the pre-examiners, Prof. Piskunov and Dr. Huovelin for finding time in their busy schedules to read through this thesis and for giving comments, and Dr Ralf Napiwotzki for acting as my opponent. I have received a lot of funding from the Finnish Graduate School in Astronomy and Space Physics, for which I am deeply grateful.

En olisi tässä ilman vanhempiani ja siskoani. Tiedän, että en sano tätä tarpeeksi usein, mutta olette minulle tärkeitä ja rakastan teitä hyvin paljon.

I grew up with a great bunch of friends. Thank you Arttu, Henrik, Pekka, Timo, Tuomas and Yukio for being there. We had a lot of fun together and I hope we will have good times together in the future too.

During my years in Turku I have met dozens of fantastic people who have made my life truly worth living. Thanks to you I am still (relatively) sane. Apart from studying/working on my PhD I have spent my days playing games, wondering around in forests and dancing Argentinian tango. Unfortunately I cannot write all your names here, but to mention a few

special friends, I want to thank Marzieh, Simo, Pauli, Jaakko, Jere, Karri, Mari, Hanna, Sandra, Nazlı, Minnamari and Mikko, Laura and Antti, and last but not least, Michelangelo and Silvia. I have spent numerous hours enjoying my life with you. I consider myself extremely lucky to have you in my life.

And finally, a very special thank you to Marianne for everything.

Tommi Vornanen,
Turku, 2013

Contents

Abstract

This thesis summarizes studies of a class of white dwarfs (WDs) called DQ WDs. White dwarfs are the remnants of ordinary stars like our Sun that have run out of nuclear fuel. WDs are classified according to the composition of their atmosphere and DQ WDs have an atmosphere made of helium and carbon. The carbon comes in either atomic or molecular form and in some cases the strong spectral absorption features cover the entire optical wavelength region.

The research presented here utilizes spectropolarimetry, which is an observational technique that combines spectroscopy and polarization. Separately these allow to study the composition of a target and the inhomogeneous distribution of matter in the target. Put together they form a powerful tool to probe the physical properties in the atmosphere of a star. It is espacially good for detecting magnetic fields.

The papers in this thesis describe efforts to do a survey of DQ white dwarfs with spectropolarimetry in order to search for magnetic fields in them. Paper I describes the discovery of a new magnetic cool DQ white dwarf, GJ841B.

Initial modeling of molecular features on DQ WDs showed inconsistencies with observations. The first possible solution to this problem was stellar spots on these WDs. To investigate the matter, two DQ WDs were monitored for photometric variability that could arise from the presence of such spots. Paper II summarizes this short campaign and reports the negative results.

Paper III reports observations of the rest of the objects in our survey. The paper includes the discovery of polarization from another cool DQ white dwarf, bringing the total of known magnetic cool DQs to three. Unfortunately the model used in this thesis cannot, in its present state, be used to model these objects nor are the observations of high enough spectroscopic resolution to do so.

List of papers

This thesis consists of a review of the subject and the following original research articles:

I **GJ 841B – The Second DQ White Dwarf with Polarized CH Molecular Bands**,
T. Vornanen, S.V. Berdyugina, A.V. Berdyugin, and V. Piirola, ApJL **720**, 52 (2010).
[arXiv:1008.3903]

II **Photometry of two DQ white dwarfs. Search for spots**,
T. Vornanen, A.V. Berdyugin, A&A **554**, L6 (2012).
[arXiv:1208.0171]

III **Spectropolarimetric observations of Cool DQ White Dwarfs**,
T. Vornanen, S.V. Berdyugina, A.V. Berdyugin,
A&A **557**, A38 (2013).
[arXiv:1308.4505]

Chapter 1

Introduction

1.1 Introduction

Dying is the faith of all living things. And so it is with stars as well. And like some people, some stars will go out in a blaze of glory as a magnificent supernova that shines brighter than an entire galaxy. But most stars, just like most people, end their days in a less spectacular way. Unlike people, however, the death of a star does not spell the end of its life.

After a star has spent its nuclear fuel and cannot maintain fusion reactions anymore, it turns into a hot ball of degenerate gas called a white dwarf (WD). This is the afterlife form of 98 % of all stars. The lifespan of a star is connected with its mass, and stars with a low mass live for a very long time (up to 10^{11} years while the universe is only 13.7×10^9 years old) and most stars have not reached the WD stage of their lives yet. Only fairly massive stars (one solar mass or more) have had enough time to evolve to white dwarfs, as well as stars in binary systems, which evolve at a different pace because of binary interactions.

The days of stars as white dwarfs are quite boring. White dwarfs do nothing but radiate their stored heat slowly into space cooling down and turning ever dimmer as the years roll by.

But even if white dwarfs are quite boring compared to younger stars, their study is still immensely important since they can tell us a lot about the evolution of stars, especially the stages of evolution that led to a white dwarf.

The degenerate state of a white dwarf core means that a large mass can be compressed into a very small space. An average white dwarf has a mass of roughly 0.6 $M_\odot$ compressed into a sphere of radius of about 10000 km, which is roughly the size of Earth. This leads to high gravity

with the consequence that pressure and temperature in the white dwarf are extremely high. These properties make white dwarfs also excellent laboratories of extreme conditions in which to test various physical theories.

White dwarfs come in many flavors and they are classified into groups by the atmospheric components that are the strongest in their optical spectra. In this thesis the class DQ is studied. These WDs are characterized by the atomic and molecular spectral features of carbon. This class is further divided into four subclasses who all have very different physical properties, and thus spectra. The hottest stars show absorption lines of ionized carbon. Cooler objects have lines of neutral carbon in their spectra, and in even cooler objects carbon forms molecules and their wide absorption bands dominate the spectra. In the coolest objects the absorption bands cover the entire optical wavelength range forming a single complex absorption feature.

Magnetic fields are a common feature on many astronomical objects. Many white dwarfs have been found to be magnetic and they contain magnetic fields as large as 10000 teslas (or 100 megagauss) but the fraction of magnetic DQ white dwarfs among all DQ WDs is largely unknown, mostly because an exhaustive survey has not been done before. This kind of a survey is at the heart of this thesis.

Chapter 2

Nature of Polarization

2.1 Polarization

Polarization is an important property of light, because it contains additional information about the source of light and the medium through which the light has travelled before reaching us. The electric field of a single wave of light can be split into two orthogonal components that are also orthogonal to the direction of propagation of the wave. The directions of the two components are arbitrary as long as they are orthogonal to each other. In Figure 2.1 the wave moves in the z-direction and is decomposed into two parts along the x- and y-axis, respectively. The electric field vector of the wave at every point along the wave is the vectorial sum of the two component waves. The polarization property of light is determined by the behaviour of the electric field vector as a function of time as the wave moves through a fixed plane. It has to be noted here that the decomposition of the wave is only mathematical and physically there is just one electric field with a direction of oscillation that can remain constant (linear polarization) or vary as a function of time (elliptical polarization).

In a general case the amplitudes of the two components do not have to be equal and the phase difference between the two components is arbitrary. If either of these conditions is met, the electric field vector draws an ellipse if viewed from the direction of propagation. This kind of light is called elliptically polarized light.

There are also two special cases of polarization called linear and circular polarization (See Figure 2.1). In linear polarization the two components are in phase and the resultant electric field vector draws a line. The direction of the line is determined by the relative amplitudes of the two components.

In circular polarization the amplitudes of the two components are equal

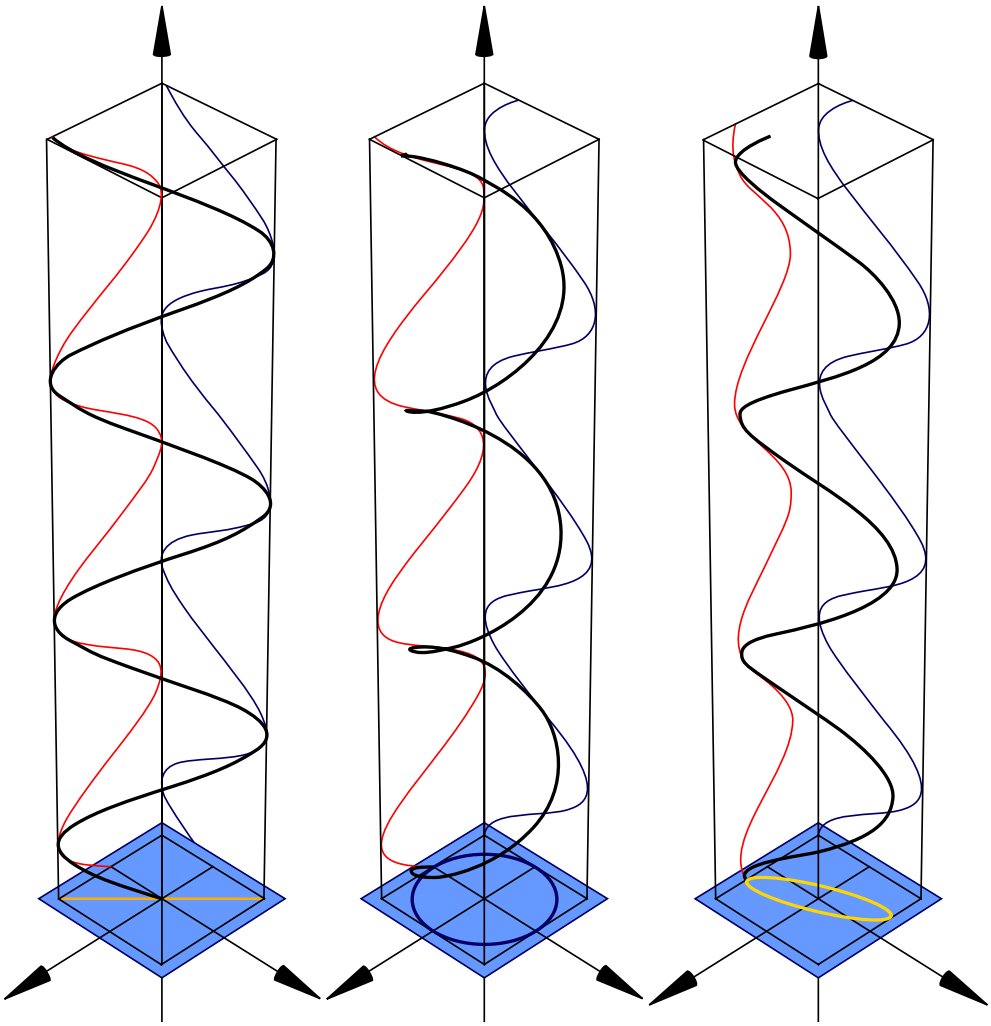

Figure 2.1: Three types of polarization: Linear, circular and elliptical. *Image Source: Wikipedia: Electromagnetic radiation.*

and they have a phase difference of exactly 90 degrees, which leads to the electric field vector rotating in a circle. There are two ways in which this phase difference can manifest itself: component x can be either 90 degrees ahead or behind component y. These two cases are called right-handed circular polarization and left-handed circular polarization depending on which way the electric field vector is rotating. Here lies a problem, however. The naming convention varies from one field of research to another.

The handedness of circular polarization of a radiation source can be determined by pointing a thumb in the direction of propagation of the wave and observing which way the other fingers curl. The hand you use then tells the handedness of polarization. The problem is that the hand you use depends on the point of view. It is different if one looks from the point of view of the source at the radiation moving away or from the point of view of the observer looking at the light coming towards himself. In electronics, quantum physics and sometimes in radio astronomy the point of view is that of the observer and in optical astronomy it is that of the source.

The total polarization of an object is the sum of the individual polarization states of all photons coming from the source. In practice the electric fields of the photons are usually randomly distributed and as a result the light is "unpolarized", which means that all directions of oscillation and both circulation directions are equally present in the light beam.

In some cases, however, the electric field vectors are not randomly oriented and some direction or one direction of circulation is more common than the others. Then the radiation coming from an object is said to be polarized. The polarization is never total, so only a part of the photons coming from a source have their electric fields aligned. *The degree of polarization* tells how much of the incoming light is polarized.

2.1.1 Sources of Polarization

The reason of the randomness of the directions of electric field vectors is the randomness of the orientation of the emitting and absorbing particles that are the source of EM radiation. Sometimes the source particles are not completely random but there is some order in their orientations. In these cases the light from the source is polarized. This ordering of particles can happen is different ways.

One way is collisions with a stream of particles. Such collisions have

the tendency to align bigger particles in the stream in such a way that the bigger particles feel as small a force from the streaming particles as possible. This same thing can be achieved by a stream of photons. If the aligned particles are structurally similar, they then scatter light in a way that the scattered light is polarized. This phenomenon can be used to study interstellar dust grains or circumstellar dust disks, for example.

Magnetic fields are a common phenomenon that causes the alignment of charged particles and thus many polarization models involve magnetic fields. The easiest way to produce polarized radiation with magnetic fields is to have free charged particles, like electrons, move in a magnetic field. The particles produce cyclotron/synchrotron radiation and since all the particles with the same sign of charge move in the same direction with respect to the magnetic field, they produce similar light. When this situation is viewed along the magnetic field lines the electrons seem to move on circular orbits and so the observed light is circularly polarized and when viewed from the side the electrons seem to all move in the same direction and the light they produce is thus linearly polarized (See Figure 2.2).

The most important effect of magnetic fields to astrophysical studies, however, is the polarization of spectral lines. The study of spectral lines gives us accurate information about the source of radiation, and the polarization properties of spectral lines in the presence of a magnetic field give us even more information about the emitting or absorbing particles and the conditions in which they are. Landi Degl'Innocenti & Landolfi (2004) contains a mathematical description of polarization effects in spectral lines including quantum mechanical calculations of the Zeeman effect.

2.1.2 Interlude: Faraday Rotation

Before light can reach the observer's instrument it has to pass through intergalactic and/or interstellar space as well as Earth's atmosphere. The "vacuum of space" and Earth's atmosphere are full of free electrons and magnetic fields and these affect light moving through them. Their effect on light is called Faraday rotation and it causes a phase difference between the left- and right-handed polarizations thus rotating the plane of linear polarization while leaving the circular polarization unmodified. The formula for this rotation is well known (Bradt, 2008) and it has a strong wavelength

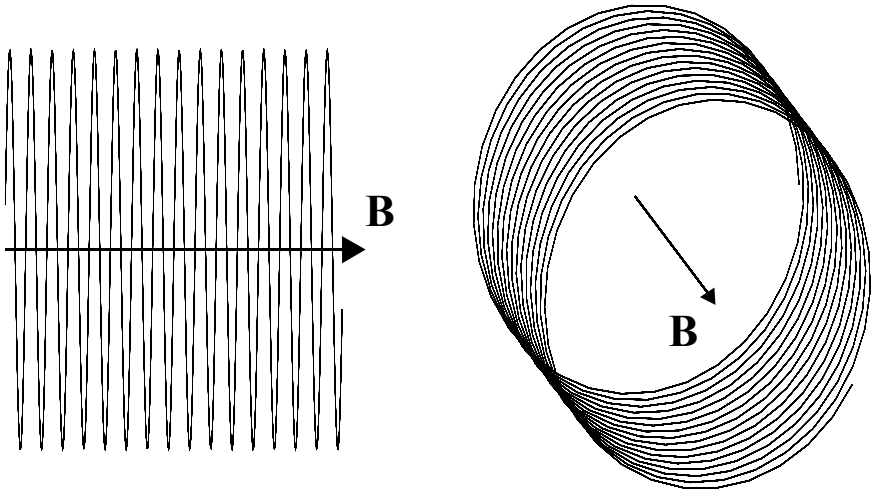

Figure 2.2: Electron moving in a magnetic field (**B**) of a helical trajectory produces polarized light depending on the viewing angle. Linear to an observer viewing the trajectory from the side and circular to an observer looking down the axis of the trajectory.

dependence:

$$\beta = RM\lambda^2 \tag{2.1}$$

where β is the angle by which the plane of polarization is rotated, λ is wavelength and RM is the rotation measure and it is given by the expression

$$RM = \frac{e^3}{8\pi^2\epsilon_0 m^2 c^3} \int_0^d n_e(s) B_{||}(s) ds \tag{2.2}$$

where n is the density of particles along the path and $B_{||}$ is the line-of-sight component of magnetic fields along the path. The other quantities have their usual meanings and this formula is to be used with SI-units (there is an alternative form to be used with cgs-units). Mass m is the mass of the charged particles, usually electrons.

The strong dependence on wavelength means that Faraday rotation is negligible for short wavelengths like optical and infrared radiation but in radio astronomy it is very important and Earth's ionosphere alone can turn the plane of polarization over 360 degrees for wavelengths of one meter. More information of Faraday rotation can be found e.g. from Bradt (2008).

2.1.3 Stokes Parameters

To study polarization and to compare results from different targets, a way to quantify polarization is needed. The most convenient way to achieve this is through the Stokes parameters introduced by George Gabriel Stokes in 1852. The four Stokes parameters are, I, Q, U, and V, and they contain information about the intensity (I), linear polarization (Q and U) and circular polarization (V).

The Stokes parameters can be defined in several ways, some of which can be found in Tinbergen (1996). The most convenient way of presenting Stokes parameters in observational astronomy defines the parameters as follows:

$$I = I_0 + I_{90} \tag{2.3}$$
$$Q = I_0 - I_{90} \tag{2.4}$$
$$U = I_{45} - I_{-45} \tag{2.5}$$
$$V = I_{rc} - I_{lc} \tag{2.6}$$

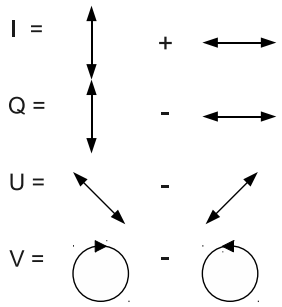

Figure 2.3: Schematic representations of the Stokes parameter. Figure adapted from Landi Degl'Innocenti & Landolfi (2004)

where the different parameters are calculated from intensities in different directions. The numbers refer to directions in an arbitrary reference frame determined by the measurement system. For circular polarization lc and rc refer to left-handed and right-handed circular polarization. A Stokes vector is a four component vector composed of the Stokes parameters. A schematic representation of these equations can be seen in Figure 2.3. Stokes parameters have the advantage that Stokes vectors of two different sources can be summed normally, for example the vectors of a background object and a cloud of gas in front of it.

Usually quantities $P_Q = Q/I$, $P_U = U/I$ and $P_V = V/I$ are used out of convenience. They are called normalized Stokes parameters and they represent which fraction of the total intensity is polarized in which way. They are unitless numbers, and as such they are easy to use. Finally, the degree of linear polarization (P_L) and the polarization angle (PA) are given by

$$P_L = \sqrt{P_Q^2 + P_U^2} \tag{2.7}$$

$$PA = \frac{1}{2} \arctan \frac{P_U}{P_Q} \tag{2.8}$$

and the degree of circular polarization is just P_V

2.2 Observing Techniques

Measuring the polarization properties of an object requires the measurement of intensity in two orthogonal directions. This corresponds to the idea of decomposing light's electric field into two orthogonal components presented in Section 2.1 and then measuring the intensities of these two components separately. Combining the relative intensities of the two components as presented in Equations 2.3–2.6 then gives us the Stokes parameters of the observed light and allows for the calculation of degrees of circular and/or linear polarization and the polarization angle.

The following paragraphs describe a way of making (spectro)polarimetric observations with a common instrument setup used in many telescopes around the world. FORS on the VLT (Saviane, 2011; Appenzeller et al., 1998) is a good example of this kind of an instrument. The intrument is attached to the Cassegrain focus of the telescope allowing for a straight optical path from the secondary mirror to the CCD. Necessary optical components, like filters, masks and grisms (grated prism) are then inserted into this path depending on the type of observations one wishes to perform. Lenses are used to collimate the beam when necessary. Plane mirrors are avoided because they cause instrumental polarization.

Making polarization observations in the optical wavelength range requires two extra optical elements in the optical system of an instrument. These are called a retarder and an analyzer, or polarizer. The former is used to control the state and direction of polarization of the light beam and the latter is used to separate the light beam into two orthogonally polarized beams. In addition to these two elements, the optical system has all the other parts necessary for photometry or spectrometry, like mirrors, lenses, prisms, and spectroscopic slits.

Traditionally, the two polarization directions have been separated by using an absorbing polarizer that lets only one polarization direction through, e.g. a Polaroid^{TM}filter. A modern analyzer is usually a beamsplitting element that separates light into two orthogonally polarized beams. The analyzer is made of a birefringent material where the refractive index n depends on the direction of the electric field vector of light. Calcite ($CaCO_3$) is the material of choice for an analyzer and they come in many forms that guide the two beams in different directions. The most common forms are a simple rod of calcite and a Wollaston prism, which consists of two calcite prisms cemented together. A beamsplitting analyzer allows the recording

of both orthogonally polarized beams simultaneously, which saves precious observing time. The two orthogonally polarized images or spectra in a single exposure caused by a beamsplitting analyzer are sometimes called the extraordinary and ordinary beams although these names more correctly refer to the beams only inside the analyzer.

There are two different kinds of retarders, or wave plates, and they are used to turn circularly polarized light into linearly polarized light or turn the position angle of linearly polarized light. The first task is accomplished by a quarter-wave plate. It introduces a $\pi/2$ phase difference between the two orthogonal components of an electric field that were discussed in Section 2.1. This has the effect of changing circularly polarized light into linearly polarized light and vice versa.

The other kind of retarder is called a half-wave plate and introduces a π phase difference between the two orthogonal components of an electric field that were discussed in Section 2.1. This changes the position angle of linear polarization and changes left-handed circular polarization to right-handed and vice versa. The retarders work by slowing the speed of light differently for the two polarization directions.

The retarders are used to control the direction of polarization in the optical system so that images or spectra at certain angles of polarization can be taken. Images at different polarization angles are needed to eliminate those instrumental polarization effects that are caused by differences between the throughput and detector sensitivity for the two beams.

The passage of light and its Stokes parameters through the optical system can be tracked with Mueller matrices (Shurcliff, 1962). A Mueller matrix describes the effect an optical instrument has on the light, more specifically the Stokes parameters of light, passing through it. The Mueller matrices of each component in the optical system can be multiplied, using matrix multiplication, to get the effect of the total system on the light passing through it. See for example del Toro Iniesta (2003, Sections 4.5 and 4.6) for an introduction to Mueller calculus.

In circular polarization observations, exposures are usually taken at two angles of the quarter-wave plate 90 degrees apart. This yields four images or spectra in total that are combined to get a Stokes V/I image or spectrum of the target. The spectra or images can be combined in different ways depending on the instrument but they are all equivalent. For example, the FORS manual for European Southern Observatory's VLT telescope (Saviane, 2011) recommends to use the following formula for calculating

Stokes V/I:

$$\frac{V}{I} = \frac{1}{2}\left[\left(\frac{f^o - f^e}{f^o + f^e}\right)_{\theta=45} - \left(\frac{f^o - f^e}{f^o + f^e}\right)_{\theta=-45}\right] \tag{2.9}$$

where f are the fluxes or spectra of the extraordinary and ordinary beams. The angle θ is the position angle of the quarter-wave plate. ALFOSC instrument on the Nordic Optical Telescope (http://www.not.iac.es/instruments/alfosc/), on the other hand, uses formulae:

$$\frac{V}{I} = \frac{1}{2}\left[\left(\frac{Q_{45} - Q_{-45}}{Q_{45} + Q_{-45}}\right)\right] \tag{2.10}$$

where $Q = E/O$ is the ratio of the extraordinary and ordinary beams and 45/-45 denotes the position angle of the quarter-wave plate. Calculating Stokes Q and U goes along similar lines but the number of combined images or spectra is 4, 8 or 16. The more images used, the less instrumental effects caused by throughput and sensitivity differences of the two beams remain in the final image or spectrum.

There is a handy formula to check whether polarization features in a Stokes V/I spectrum are real or instrumental. Bagnulo et al. (2012) give a formula for the so called null profile. In most cases it reduces polarization from natural sources in the spectrum to zero leaving only instrumental sources of polarization. The null profile can be calculated from

$$N_V = \frac{1}{2}\left[\left(\frac{f^o - f^e}{f^o + f^e}\right)_{\theta=45} - \left(\frac{f^o - f^e}{f^o + f^e}\right)_{\theta=-45} - \left(\frac{f^o - f^e}{f^o + f^e}\right)_{\theta=225} + \left(\frac{f^o - f^e}{f^o + f^e}\right)_{\theta=135}\right]. \tag{2.11}$$

Unfortunately, observers rarely use all four angles of the retarder when they do circular polarimetry. But the same thing can be achieved by calculating Stokes V/I from two consecutive sets of two images using Equation 2.9 and subtracting the second from the first. This cuts out all long lasting sources of polarization and leaves only changes that happen within the timescale of 4 exposures. These short variations should be from the imaging system, but for long exposures it is possible that the target can change too. So caution needs to be exercised when using this method.

There are a couple of things that have to be taken into account when

planning and performing polarimetric or spectropolarimetric observations. Flux calibration is done just like in normal photometry or spectroscopy comparing to other field stars or observing the spectrum of some known object. For the calibration of polarization a couple of standards are needed. These are zero-polarization standards and high polarization standards. Observations of circular polarization are different from linear polarization observations in the required standards.

The modern instruments capable of circular spectropolarimetry have no instrumental polarization, at least not at the accuracy limit of the observations, so a zero polarization standard is not necessary. A known high polarization standard is needed to calibrate the sign of circular polarization. In the southern sky no such standard is known as of yet, but the white dwarf G99-37 has a strongly polarized feature at roughly 430 nm, which can be used to calibrate the sign (Berdyugina, Berdyugin & Piirola, 2007). In the northern hemisphere a WD called Grw +70 8247 can be used as a high polarization standard.

In linear polarimetry more standards are needed. Instrumental polarization can be a problem, so a zero-polarization standard is required. Also two high-polarization standards are needed to calibrate the position angle of linear polarization. Fortunately there are plenty of objects with known polarization properties.

One important thing to consider when planning observations is the accuracy of polarization measurement. The accuracy in the polarization spectrum or an image can be estimated with

$$\sigma_P = \frac{\sqrt{2}}{\sqrt{n} \times S/N} \tag{2.12}$$

where n is the number of wave plate positions. For example a signal-to-noise ratio (S/N) of 300 gives $\sigma_P = 0.005$ for circular spectropolarimetric observations with two quarter-wave plate angles. This is not much considering that polarization rarely exceeds 1%. The above formula uses the combined S/N in both beams, which can be difficult to estimate. If the S/N of each beam is known, then the error is given by

$$\sigma_P = \frac{1}{\sqrt{n} \times S/N}. \tag{2.13}$$

In this case the accuracy of $\sigma_P = 0.005$ requires S/N to be 150 in both

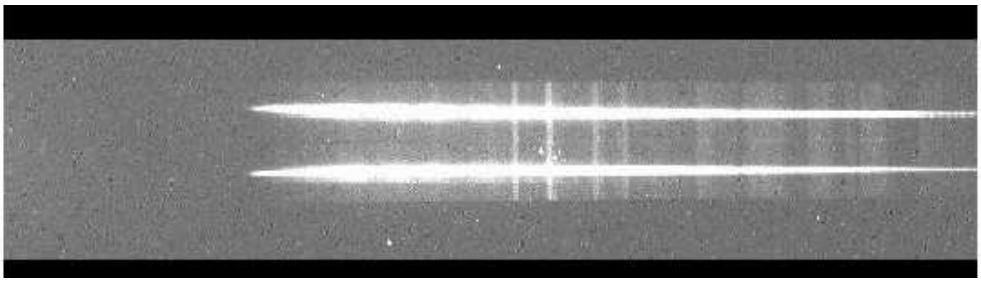

Figure 2.4: Raw image from a spectropolarimeter.

beams for circular (spectro)polarimetry with two wave plate angles.

2.2.1 Data Reduction

Data reduction of polarimetry follows the same principles as photometry and spectrometry. Starting point is a raw image provided by the instrument (Figure 2.4). Note that the example presented here is spectropolarimetry and important differences to photopolarimetry are pointed out.

Data reduction starts with a bias subtraction to remove the zero level flux from the CCD electronics. Next, some sort of automated or manual cosmic ray removal is in order. Especially for big telescopes and long exposures, the amount of cosmic rays can reach large numbers and their presence can be seen in the final spectra if not correctly removed.

Next reduction stage is usually flatfielding, which is used to correct for pixel-to-pixel variations and in the case of (spectro)polarimetry the differences in transmission of the two orthogonally polarized beams in the optical system. However, the pixel-to-pixel variations are mitigated by the common use of 2x2 binning when the CCD is read after an exposure and the high quality of modern CCDs. The second problem is corrected by calculating the degree of polarization from two or more consecutive exposures whit different retarder plate angles. This effectively cancels all sensitivity differences. For these reasons flatfielding is not necessary for spectropolarimetric observations (Bagnulo et al., 2009, 2012).

Background subtraction is an important step in any data reduction. In spectropolarimetry background has to be subtracted separately for both beams. In practice this happens by calculating an average (or median)

background value on both sides of one beam and subtracting this from the image. Then the same is done for the other beam. This results in two images for every bias and cosmic ray corrected image. The background level around the spectrum should be zero after this step. This step together with combining two or more images to calculate the Stokes parameters efficiently removes all sources of background polarization caused by the sky including clouds and the Moon. It also removes atmospheric emission lines visible in Figure 2.4.

Next, the two spectra have to be extracted from the image. A data reduction package like IRAF (Tody, 1993) finds the peak value in each column (once the rough position of the spectrum has been indicated) and then the user has to choose one of two methods. The first involves a fixed width window within which all flux is added together in each column. Width of this window is naturally determined by the widest part of the spectrum. This method will include some flux from the background but since this has been reduced to zero on average by the previous steps, very little residual from the sky should remain and all flux will be included in the spectrum. In the other method a limiting flux is chosen and, starting from the peak flux, in each column the flux is added from both sides of the peak until the limit has been reached. This limit can be set to, for example, 3 % of the peak flux. This method assures that there is no unnecessary background in the extracted spectra but some flux is discarded by the process, which is usually undesirable when the target is very faint.

After the spectra have been extracted, they need to be wavelength calibrated. This is done by assigning wavelength values for pixels by looking at a spectrum of a calibration lamp and comparing to a similar image with emission lines identified with their correct wavelengths. When a good solution is found, the wavelength-pixel correspondence information has to be attached to the headers of the spectrum files. Note that this procedure has to be done for both beams separately as the two beams tend to be slightly shifted in the dispersion direction with respect to one another. After this procedure the extraordinary and ordinary spectra are ready for polarization calculations.

The reduced spectra are used to calculate the Stokes parameters. Linear polarization data need one more calibration step, though. The instrumental position angle (PA) has to be determined from the high polarization standards and added to the science targets. This is done by first calculating

the PA for the high polarization standards using Equation 2.8

$$PA_{measured} = \frac{1}{2} \arctan \frac{P_U}{P_Q}, \tag{2.14}$$

then comparing their values for literature values

$$PA_{correction} = PA_{true} - PA_{measured}. \tag{2.15}$$

This correction can then be used to determine the corrected values for $P_U = U/I$ and $P_Q = Q/I$ using equations from Bagnulo et al. (2009)

$$P_{Q,c} = P_Q \cos(2 \cdot PA_{correction}) - P_U \sin(2 \cdot PA_{correction}) \tag{2.16}$$
$$P_{U,c} = P_Q \sin(2 \cdot PA_{correction}) + P_U \cos(2 \cdot PA_{correction}) \tag{2.17}$$

After this the corrected P_Q and P_U values are used for calculating the final degree of linear polarization using Equation 2.7

$$P_L = \sqrt{P_{Q,c}^2 + P_{U,c}^2}. \tag{2.18}$$

Polarization observations are more complicated than intensity observations (either imaging to spectroscopic) so why should one care about polarization? The answer is simply that the amount of information contained in the Stokes parameters (or any other system describing the polarization properties of objects) is far greater than in regular intensity observations. By using polarization it is possible to detect magnetic fields with much more sensitivity due to the polarization properties of the Zeeman effect, for example. In general, polarization contains information about the geometry of an object that could not otherwise be determined.

Using polarization naturally has a downside as well. The magnitude limit for polarimetric observations is much lower than for intensity observations. For example, using the FORS2 instrument (Appenzeller et al., 1998), allows to do low resolution spectropolarimetry on targets of visual magnitude $\sim$18 in one night, whereas similar observations without polarization can go one magnitude deeper. But intensity observations rarely need the high S/N that is required to get a good accuracy in Stokes parameters, so even fainter objects can be studied with intensity observations.

Chapter 3

White Dwarfs

White dwarfs are the remnants of low mass stars. Current evolutionary models tell us that stars with initial masses between 0.5 $M_\odot$ and 8 $M_\odot$ end their lives as white dwarfs. It is easy to calculate from the Salpeter initial mass function (IMF) (Salpeter, 1955) that roughly 98 % of all stars end their life as a WD (See for example Kawaler, Novikov & Srinivasan, 1997, for details on the derivation). White dwarfs studies are important for several reasons. They are good laboratories for extreme conditions like high temperatures and strong gravity because they have a relatively simple structure. They also cool in a simple manner making it possible to estimate their ages. This in turn can be used to limit the age of stellar groups, galaxies and the age of the Universe itself. White dwarfs in binary stars are host to some interesting phenomena which allow the study of binary evolution and the evolution of the secondary stars in binaries. Finally, rare double WD binaries are sources of gravitational radiation and very important for future studies of gravity.

The following outline of white dwarfs' evolution is based largely on Kawaler, Novikov & Srinivasan (1997).

3.1 Evolution From Giant to Dwarf

Low and intermediate mass stars end their lives as normal stars on the asymptotic giant branch (AGB). At that point they have exhausted their supply of nuclear fuel in the core and gone through several evolutionary phases as giant stars. In an AGB star hydrogen and helium continue burning in layers so that the core of carbon and oxygen stays relatively stable. On top of this stable core that will become the core of the white dwarf,

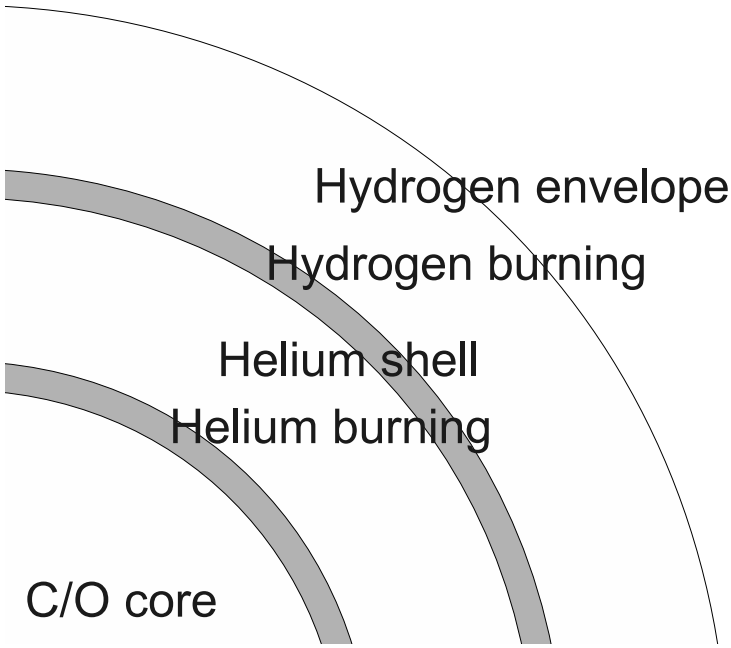

Figure 3.1: Internal structure of an AGB star

there is a layer where helium is going through nuclear fusion transforming into carbon and oxygen. This layer is fueled by a shell of helium on top of it. On top of this helium shell is a layer where hydrogen is burning into helium fueled by an envelope of hydrogen on top of it. Figure 3.1 illustrates this layered structure of an AGB star.

AGB stars are very large, up to 1.5 AU in radius and also very luminous ($L \simeq 10^3 - 10^4 L_\odot$) (See Herwig, 2005, for a review on AGB stars). The hydrogen and helium burning layers alternate as the energy source of the star and this late phase in stellar evolution is characterized by strong mass loss, up to $10^{-4} M_\odot$/year. The surface temperature of an AGB star is low, only 3000–5000 K, and molecules and dust grains can form in its envelope.

For most of its lifetime, an AGB star is burning hydrogen into helium at the bottom of the envelope. This helium sinks into the helium shell. When there is enough helium in the shell, temperature and pressure at the bottom

of the shell are high enough for helium to start fusing into carbon. This causes a sudden rise in radiation pressure and the envelope is blown out and the star's diameter grows significantly. At the same time the envelope cools and the simultaneous drop in temperature and pressure stops the hydrogen burning.

When most of the helium has been turned into carbon, the radiation pressure drops and the hydrogen envelope can shrink back in rising the temperature and pressure at the bottom of the envelope, and so hydrogen burning starts again. This cycle repeats for $5 \times 10^5 - 10^6$ years with 10^5 years between the helium flashes. The helium burning phase lasts only about 400 years.

During the above process, the envelope mass is decreasing constantly because of a stellar wind and also because of hydrogen fusion at the bottom of the envelope. The effective temperature of the star is a very weak function of the envelope mass for most of this time but when the envelope mass gets down to about 0.001 $M_\odot$ the situation changes and any loss of envelope mass leads to large increases in effective temperature (Schoenberner, 1983). At this point, the white dwarf core of the star has been exposed and the rapid increase in temperature moves the star left on the Hertzsprung–Russell diagram.

If this increase in temperature happens during the hydrogen burning phase, the WD will have a hydrogen atmosphere. If the departure from asymptotic giant branch happens when the star is close to starting another helium flash, the star can undergo this flash after leaving the AGB. In this case the flash moves the star briefly back to the AGB phase which leads to an episode of mass loss through a stellar wind and the star loses almost all hydrogen and the resulting WD will have a helium dominated atmosphere (Iben, 1991).

If the departure from AGB happens during the helium flash or shortly after it, there is very little or no hydrogen at all in the outer layer of the star and the white dwarf will have a helium atmosphere. Iben (1984) estimated that 20 % of white dwarfs leave the AGB in the helium burning phase or shortly after it and that is the reason why 20% of WDs have helium atmospheres.

After leaving the AGB phase the pre-WDs have surface temperatures of the order of 10^5 K and the intense radiation from the exposed hot core ionizes the expelled material that is still around the star and the result is a planetary nebula. The ionization can happen only if the surrounding gas is

optically thin, and this is not the case in all objects. Still, a vast majority of all known pre-WDs are in planetary nebulae, because planetary nebulae are very easy to find.

All this time, the core of the AGB star is composed of a mixture of carbon and oxygen. The force preventing further collapse is electron degeneracy, which means that electrons have filled the phase space almost completely and electrons can move relatively freely within the core. The transition from AGB star to WD does not affect the core in any way.

After the planetary nebula phase the white dwarf cools down. This is a slow process taking billions of years as the thermal energy stored in the core of WD slowly dissipates into space. The process is slow because the core is small and it is covered by an atmosphere that acts as a blanket very effectively preventing heat loss. An expression for how long it takes for a WD to cool to a given luminosity can be derived (again, details can be found in Kawaler, Novikov & Srinivasan, 1997) and the expression is:

$$t_{cool} = 9.41 \times 10^6 \mathrm{yr} \left(\frac{A}{12}\right)^{-1} \left(\frac{\mu_e}{2}\right)^{4/3} \mu^{-2/7} \left(\frac{M}{M_\odot}\right)^{5/7} \left(\frac{L}{L_\odot}\right)^{-5/7} \quad (3.1)$$

where A is the atomic weight of the core material (12 for carbon, 16 for oxygen and 14 for a 50/50 mixture of carbon and oxygen), μ_e is the mean molecular weight per electron in the core and μ is the mean molecular weight of the envelope. It can be seen from the formula that cores composed of lighter elements will fade more slowly than cores composed of heavier elements, like neon. Also, more massive WDs cool and fade slowly compared to less massive WDs.

Two additional effects that have to be taken into account in models of WD cooling are neutrinos and crystallization. These effects alter the cooling curve of the above equation only slightly.

The discussion so far has only concerned single stars. Another way of producing white dwarfs is provided by binary evolution. A large portion of known white dwarfs are in binaries and they are known as cataclysmic variables. The interaction with the companion star greatly alters WD evolution in these objects.

3.2 Atmosphere

Average mass of a white dwarf is 0.6 M$\odot$ (Tremblay, Bergeron & Gianninas, 2011) but the radius of a WD is only of the order of 10000 km. The radius is an inverse function of mass: the larger the mass, the smaller the radius. What makes a WD atmosphere so interesting is that the temperature at the bottom of the atmosphere is $\sim 10^7$ K but the surface temperature is between 150000 K and 4000 K. This, coupled with a very thin atmosphere, makes WDs very interesting subjects to study.

All the spectral features we see on a WD are from the atmosphere and these features can be used to divide WDs into classes. As was described in the previous section, the main atmospheric component is determined by the stage in which the star is when it leaves the AGB phase of evolution. After this the strong gravity leads to gravitational settling of elements in the atmosphere. Heavier elements like carbon sink deeper while lighter elements, helium and hydrogen, rise to the top forming a layered structure. The top layer then determines the observed properties of a WD and has led to a classification system.

For historical reasons the classification scheme for white dwarfs is based mostly on optical spectra. After all, optical region was the first to have working spectrographs. The two main classes of WDs are called DA and DB. The letter D stands for degenerate telling that these are true dwarfs. DA WDs have mostly hydrogen lines in their spectra. DB WDs were originally used as a class for all non-DA WDs. Now, DB means white dwarfs that have neutral helium lines in their spectra. The use of letters A and B comes from a comparison to spectra of main sequence stars. The spectra of A stars are dominated by Balmer lines of hydrogen as are DA WDs and similarly B stars have spectral lines of neutral helium.

There are also WDs that have helium cores. These are the product of binary star evolution and they are the lightest WDs (Liebert et al., 2004). A low mass star will also turn into a helium core WD at the end of its evolution, but this process takes so long for a low mass star that no star has had time to evolve so far in the limited 13.7 billion year age of the Universe.

The DB class has several subclasses. They contain WDs that have a helium atmosphere but their spectra mostly have spectral lines from other elements than neutral helium. DO WDs are characterized by singly ionized lines of helium and perhaps represent the earlier stages of helium atmo-

sphere WD evolution. DC white dwarfs have a helium atmosphere but they are too cool to have spectral lines in their spectra.

DZ white dwarfs have metal lines in their spectrum. The source of these pollutants is thought to be accretion from interstellar material or circumstellar matter. See Koester et al. (2011) for a discussion on the present day view on the subject. Metal lines can be found in both DA and DB white dwarfs giving rise to a secondary spectral classification. For example, a DAZ WD has strong spectral features of hydrogen and weaker lines of metals, and DZA has stronger metal lines than hydrogen lines.

The most important white dwarf spectral class for this thesis is, however, the class DQ. These WDs have carbon lines in their spectra, either in optical or in other wavelength regions. The carbon can be in either atomic form or in molecules. Section 3.5 describes this class in much more detail.

In addition to the aforementioned spectral types, there are a few other letters that can be added to the classifications above to specify what kind of a WD is in question. P and H denote magnetism with P meaning there is a polarization signal detected and H meaning no polarization has been detected but magnetism has been inferred in another way. V at the end of a classification means a variable WD. In addition, X, : and ? are used if the given classification is uncertain. After any letters and symbols, the classification is followed by a number representing the surface temperature of the WD. This number comes from the simple formula 50400/T. Originally, the number was supposed to be an integer but decimal numbers are in use these days because models and observations have improved and have made more accurate temperature determinations possible.

The classification scheme presented here was introduced in Sion et al. (1983) and it has been modified slightly where necessary after its publication.

The evolution of white dwarfs as presented above utilizes different evolutionary paths to the different kinds of observed white dwarfs. There are also theories that describe WD evolution in a way where DA and DB white dwarfs are just phases in the development of all WDs and these stars would go through them no matter in which phase of AGB star evolution they left the asymptotic giant branch (Fontaine & Wesemael, 1987). Whatever the truth is, it is clear that getting to it will still require large amounts of research.

3.3 Magnetism

Magnetism in white dwarfs was found over 40 years ago (Kemp et al., 1970) and since then many white dwarfs have been found to be magnetic. WD magnetic fields show a large spread in strength, between $10^4 - 10^9$ G (1-10000 T) (Külebi et al., 2009). Despite large amounts of research done on WDs there is still no consensus on the source of magnetism in WDs. A review of single white dwarf magnetism and magnetism of white dwarfs in binaries has been done by Wickramasinghe & Ferrario (2000).

In main sequence stars there are two theories how stars can acquire their magnetic fields: dynamo action in convective layers and the so-called fossil field theory. In our Sun, and in other lower main sequence stars, the weak and complicated magnetic fields on the surface are created by a dynamo mechanism driven by convection in the appropriate layers in the atmosphere of a star. Magnetic fields in these small stars also vary on different timescales.

The magnetic fields of intermediate mass stars are a little different, however. They are well ordered (usually dipolar) and show no variability. There are some theories that exploit dynamo action as the source of magnetic fields in intermediate stars too but the prevailing theory at the moment explains the magnetic fields on these stars as a remnant from the time of the formation of the star from a molecular cloud. The fossil field theory produces fields that match the observed properties better than dynamo theories. A recent review from Donati and Landstreet (Donati & Landstreet, 2009) summarizes our current knowledge of magnetic fields on the main sequence.

A large fraction of the low mass stars observed with proper techniques have been found to be magnetic, but out of the intermediate mass stars, only a small subset, the chemically peculiar Ap/Bp stars, seems to be magnetic. Intermediate mass stars are the progenitors of white dwarfs, but there is no commonly accepted theory of how, or whether, the magnetic field survives the transition from star to WD.

The WD atmosphere is convective so a dynamo action is not ruled out, and indeed, some WDs are thought to show spots similar to those in the Sun (Valyavin et al., 2011). But it is unlikely that a dynamo mechanism could be responsible for the 100 MG fields detected in several WDs. On the other hand, if a star's magnetic field is frozen in the core of the star, its strength would grow by a factor of 10^4 as the star turns into a WD,

because a dipolar magnetic field strength has a $1/R^2$ dependence and the star's radius will shrink by a factor of 100 as it turns into a WD. This would strengthen a 10 kG field to a 100 MG field.

Magnetism in single white dwarfs manifests in two ways, splitting and polarization of spectral lines and as continuum polarization. In binaries, there often is accretion from a secondary to the white dwarf, and if the WD is magnetic, the accretion stream can be a source of cyclotron radiation (see e.g. Piirola et al., 2008), which is also polarized in addition to the line effects and continuum polarization.

In addition to splitting the energy levels of an atom or a molecule, a magnetic field influences the thermodynamic environment changing the pressure, for example. Also, a magnetic field is never truly uniform and there are small variations in its strength due to local properties. These, and other, effects contribute to the polarization of a spectral line making modelling very complicated (Landi Degl'Innocenti & Landolfi, 2004).

Continuum polarization shows the combined effect of different polarization producing mechanisms, including cyclotron radiation, from the entire atmosphere. The varying conditions across the atmosphere make polarized features broaden so much that the whole continuum ends up being polarized (Wickramasinghe & Ferrario, 2000).

3.4 Variability

There is one more important aspect of white dwarf studies that needs to be mentioned here, although it has no bearing on this thesis, namely variability. Not variability caused by rotation of the white dwarf, which comes from inhomogeneous surface features, like spots, but variability caused by pulsations.

Stars in their giant phase of evolution go through several pulsation phases, in which their radius is changed, sometimes drastically. One example is the aforementioned cycles in the AGB phase, which make the radius of a giant change. These radial pulsations usually happen in the freefall timescale of the star.

The pulsations found on white dwarfs happen in the timescale of hundreds of seconds. The first WD found to pulsate (Landolt, 1968) has a pulsation period of 720 seconds. The problem is that, because of their meager radius, the freefall timescale of a WD is about 10 seconds. Later

studies found the pulsations to be nonradial and a new class of WDs was named, traditionally, after the first known object, ZZ Ceti.

The non-radial pulsations in a WD (and other stars) are due to convection that transports non-ionized material deeper into the atmosphere where it ionizes and causes opacity changes, which lead to density changes. The strong gravity of a WD tries to restore these fluctuations, which results in pulsations. These kind of pulsations (g-mode pulsations) have been found on DA, DB, DO, and most recently on hot DQ white dwarfs (Green et al., 2009). These pulsations are important, because they allow us to study the stellar interior through asteroseismology (Romero et al., 2011). Kawaler, Novikov & Srinivasan (1997) includes a summary on the information that can be gained from WD pulsation periods.

3.5 DQ White Dwarfs

As mentioned in Section 3.2 DQ WDs are white dwarfs with carbon spectral features. The class can be further divided into 4 different subclasses based on optical spectra. Hot DQs are objects with CII lines in the spectra. Objects with CI lines do not have a name yet, but they might be called warm DQs. Cool DQs have molecular lines of C_2 and in two cases CH. Finally, there are peculiar DQs which have very distinctive spectral features, also from C_2.

Actually, atmospheres of these WDs are helium dominated, but in most cases helium lines are not present in the spectra because of low temperatures (Dufour, Bergeron & Fontaine, 2005). In non-hot DQ WDs the helium atmosphere is so thin that convection brings significant amounts of carbon up from the transition between core and atmosphere. In surface temperatures above 11000 K the carbon remains in atomic form and the spectra of these WDs shows lines of atomic carbon. When the temperature drops below 11000 K increasing amounts of carbon is found in molecular form and soon (below 9000 K) the spectrum is covered by absorption bands of C_2. These molecular bands cover the whole optical region and they are also visible in ultraviolet and near infrared parts of the electromagnetic spectrum. The molecular absorption bands in optical are almost all Swan bands with some smaller Deslandres-d'Azambuja bands mixed in (See Section 4.3). Paper III, Figure 1 shows a representative collection of spectra of cool DQs.

When the surface temperature drops below 6000 K, the carbon absorp-

tion bands meld together to form a very strong and wide absorption band and these stars are called peculiar DQ WDs (DQpec classification). It was thought for a long time that the spectral features in these stars are formed by some other carbon molecule (Schmidt, Bergeron & Fegley, 1995) but more recent studies of molecular spectra have shown that they are, indeed, from C_2 (Hall & Maxwell, 2008). Spectra of these peculiar objects can be seen in Figure 3.2.

The spectral features in the optical region in peculiar DQs are the Swan bands of C_2 but why they appear as they do is still uncertain. Some possibilities are discussed in Section 4.3. The surface temperature in peculiar DQs is thought to be $\lesssim 6000$ K (Hall & Maxwell, 2008) but this is hard to check since the strong absorption feature covering the optical range makes spectral fitting difficult and influences colors in a way that makes the overall brightness of these WDs seem less than it actually is. The absorption features themselves can be used to estimate a temperature but, as is noted in Hall & Maxwell (2008), at low temperatures helium is neutral and the visible photosphere is deep down in the atmosphere. Because of this we see the carbon molecule in a range of temperatures and pressures and thus a range of rotational excitation levels (See Section 4.3 for further discussion). Also magnetic fields can influence the shape and strength of the absorption features. It is clear that a lot of work with accurate and realistic WD atmosphere models including carbon are needed to tackle this issue.

The hot DQs are thought to be on a completely different evolutionary path than the rest of the DQ WDs. Their atmospheric temperature is between 15000 K and 24000 K and should thus show helium lines. Careful examination of the objects led Dufour et al. (2007) to conclude that the atmospheres of these WDs are strongly carbon dominated. Dufour et al. (2008) used log(C/He) and log(C/H) values between 0 and 2 to model the spectra of hot DQs. For comparison, the relative abundance of carbon in cool DQs is usually between 10^{-7} and 10^{-3} (Dufour, Bergeron & Fontaine, 2005). The above temperatures are too hot for convection to work so the carbon has to originate from the atmosphere. On the other hand, the amount of carbon is too large for having been accreted from interstellar/circumstellar material (Dufour et al., 2007).

These facts have given rise to speculations that these WDs could actually have ONeMg cores, or the progenitor AGB stars have undergone a very late thermal pulse that would have blown away most of the helium and hydrogen in the atmosphere and what is visible is actually the exposed

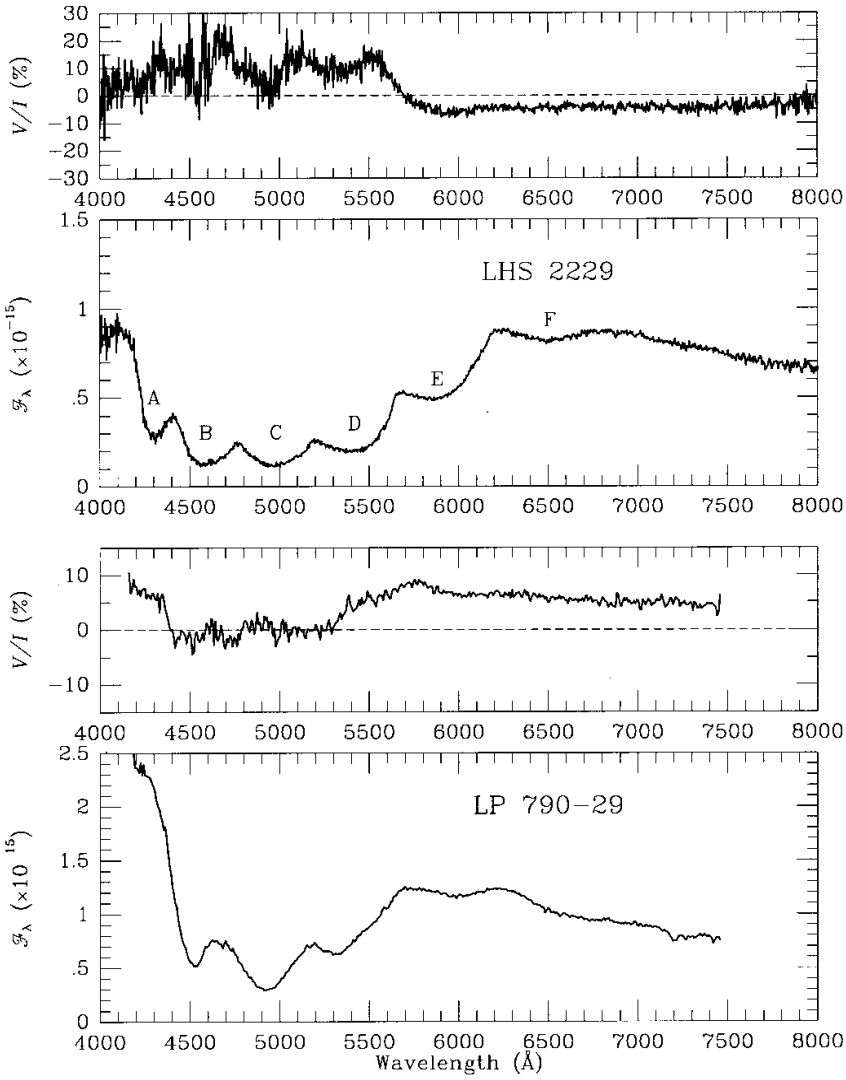

Figure 3.2: Optical Stokes I and V spectra of peculiar DQs from Schmidt et al. (1999)

core of a C/O WD. The evolutionary scenarios are discussed at length in Dufour et al. (2008). It is difficult to say what comes of the hot DQs when they cool down. Maybe they become peculiar DQs. In this case normal DQs would just loose the carbon in their atmospheres due to gravitational settling and turn into DB/DC white dwarfs as they cool down.

The class DQ WDs has magnetic members as well. Detecting a magnetic field in hot DQs is done through the Zeeman splitting of the atomic carbon lines. Dufour et al. (2010) report magnetic fields on 5 of the 14 known hot DQs with further possibility of 4 other stars being magnetic as well. This ratio (> 50 %) is extremely high compared to the 10-15 % observed in nearby WDs (Liebert, Bergeron & Holberg, 2003). It begs the question are magnetic fields somehow related to their evolution. The sample is not very large and all the objects are extremely faint ($M_V \gtrsim 18$), which makes it very difficult to say anything definite about the class.

There are 4 known magnetic peculiar DQs, which is also a high fraction of the total, although the total number of peculiar DQs is also shrouded in mystery since not all of them are tagged as peculiar in the Simbad database. The magnetic nature is deduced from the presence of circular polarization in the stellar spectra. An example of the Stokes V/I spectra of peculiar DQs can be seen in Figure 3.2. There does not seem to be any coherence in the form of the polarization signal across the optical wavelength region since the objects show very different polarization properties (Schmidt et al., 1999, 2003).

Curiously only one normal, cool DQ (G99-37) has been found to be magnetic and the discovery of a second such object is reported in Paper I. The total amount of DQs is close to 200, so there is a lack of magnetic cool DQ WDs. Paper III reports efforts of finding more magnetic DQs. An even more curious fact is that only the two magnetic cool DQs are known to show spectral features of CH (Paper I). CH reacts to the presence of a magnetic field more strongly than C_2, which might explain the coincidence, but it could also be that CH is somehow a result of the magnetic field. Until a non magnetic DQ WD with CH or a magnetic normal DQ WD without CH can be found, the question has to be left hanging in the air.

As mentioned above, some of the hot DQs have been found to be variable (Montgomery et al., 2008; Barlow et al., 2008; Green et al., 2009) experiencing non-radial pulsations. Unfortunately, the instability strip on the Hertzsprung-Russell diagram these WDs are crossing is at too high temperatures to be useful for the study of cool DQ WDs.

Photometric observations to look for variability in two cool WDs are presented in Paper II. Spots have been found on some WDs (Brinkworth et al., 2005) but our search did not give positive results for the two observed stars. Since single WDs are thought to have very long rotation periods (Schmidt & Norsworthy, 1991), observing variability due to spots or some other mechanism showing itself through the rotation of the WD is almost impossible.

Chapter 4

Molecules

After the development of quantum mechanics, the study of stars was revolutionized by spectroscopy. When the energy levels of atoms and the transitions between them could be solved analytically, and the effects of various physical phenomena to these levels and transitions could be deduced, the universe opened up to us like never before. This knowledge has made it possible to study the physical conditions in stars and galaxies, on planets and in gas, molecule and dust clouds. Soon after the energy levels of simple atoms were solved, the attention was turned to molecules.

Even molecules composed of two atoms, for example C_2 or CH, are much more complex than single atoms. But they can be described with quantum mechanics in a way similar to atoms. These calculations give the energy level structure of the molecule, as well as information about the effect of the physical environment (temperature, pressure, magnetic fields etc.) on those levels. Large amounts of molecules in the atmospheres of cool objects like M-dwarf stars, brown dwarfs and cooled down white dwarfs make them a useful diagnostic tool for studying these objects.

The following outline is based on lecture notes of a course in molecular spectroscopy given by prof. Svetlana Berdyugina at Kiepenheuer Institute für Sonnenphysik and lecture notes of a course in astronomical spectroscopy given by Dr. Juha Reunanen at University of Turku. Also Hartquist (1990) contains some of the information presented here.

4.1 Energy Levels and Quantum Numbers

Just like for atoms, the energy level structure of molecules can be solved using a Schrödinger equation and the possible transitions are determined

by a set of quantum numbers. The energies involved in molecules are, of course, more complex than for atoms and the quantum numbers are defined differently for molecules than for atoms although they both share many analogous quantum numbers.

The total energy of the molecule can be described as a sum of the energies of the electrons and the nuclei that comprise the molecule. This can be represented as a sum of three energies: electronic energy, vibrational energy and rotational energy (in descending order of strength) and the energies of their interactions.

The simplest molecule is made of two atoms and this section concerns these diatomic molecules. Even diatomic molecules are much more complicated than atoms and complexity increases with increasing number of atoms.

4.1.1 Electronic Energy

Molecules are built by bringing atoms together. The electron structure around the atomic nuclei changes due to Coulombic forces and, if the resultant combination has a lower energy, a molecule can form. The molecular energy states result from some of the states of the separated atoms.

When two atoms, which have orbital angular momenta $\overline{L}_1$ and $\overline{L}_2$ and spins $\overline{S}_1$ and $\overline{S}_2$, form a molecule, an electric field is formed between them along the internuclear axis. The field is so strong that the coupling of $\overline{L}_i$ to the field is stronger than coupling to $\overline{S}_i$.

The electric field produces a quantization of $\overline{L}_1$ and $\overline{L}_2$ in the internuclear axis direction with components $\overline{M}_{L_1}$ and $\overline{M}_{L_2}$. The electronic orbital angular momentum of the molecule is then given by the quantum number

$$\Lambda = |\overline{M}_{L_1} + \overline{M}_{L_2}|, \tag{4.1}$$

which gets values $\Lambda = 0, 1, 2, 3, 4...$ that are denoted by Greek letters $\Sigma, \Pi, \Delta, \Phi, \Gamma...$, respectively. In other words, Λ is the projection of the electronic orbital angular momentum on the molecular axis.

Spin, on the other hand is not influenced by an electric field, so the spin vectors of the atoms can be summed to give a spin vector for the molecule

$$S = S_1 + S_2, S_1 + S_2 - 1, ..., |S_1 - S_2|. \tag{4.2}$$

If $\Lambda \neq 0$ ($\Pi, \Delta, ...$ states) the orbital motion of electrons creates an internal magnetic field along the internuclear axis. The magnetic field causes $\overline{S}$ to precess around the field direction with a constant component $M_s\hbar$. For molecules M_s is denoted by Σ,

$$\Sigma = S, S-1, ..., -S. \tag{4.3}$$

The quantum number Σ is the projection of the electronic spin angular momentum on the molecular axis.

Total angular momentum of the electrons is then given by

$$\overline{\Omega} = \overline{\Lambda} + \overline{\Sigma}. \tag{4.4}$$

As both Λ and Σ are along the internuclear axis, an algebraic sum is enough to determine Ω

$$\Omega = |\Lambda + \Sigma|. \tag{4.5}$$

These quantum numbers are related to the electron structure of the molecule. To describe the whole molecule, we need to include some quantum numbers that describe the effects of the nuclei and the interactions between the nuclei and the electron cloud around them. Figure 4.1 shows these quantum numbers. There are two cases, named Hund's case a and b after their discoverer. These cases differ from each other in the coupling of the total electron spin, S, to the internuclear axis. In case a the spin is coupled to the axis and the quantum number Σ is used. In case b the electronic spin is not coupled to the internuclear axis and S is used as a quantum number instead of Σ.

R is the orbital angular momentum of the nuclei with respect to the molecule's center of mass. The vector sum of R and Ω, J, is the total angular momentum of the molecule (excluding nuclear spin). In Hund's case b the quantum numbers of nuclear angular momentum, R, and electronic angular momentum, Λ, are summed (vectorially) to get N, the total orbital angular momentum. N and S are then summed to get the total angular momentum of the molecule, J.

The spectroscopic notation of a state for a molecule is very similar to the atomic notation. The orbital angular momentum of a molecule is denoted by a Greek letter $\Sigma, \Pi, \Delta, \Phi, \Gamma...$ corresponding to $\Lambda = 0, 1, 2, 3, 4....$

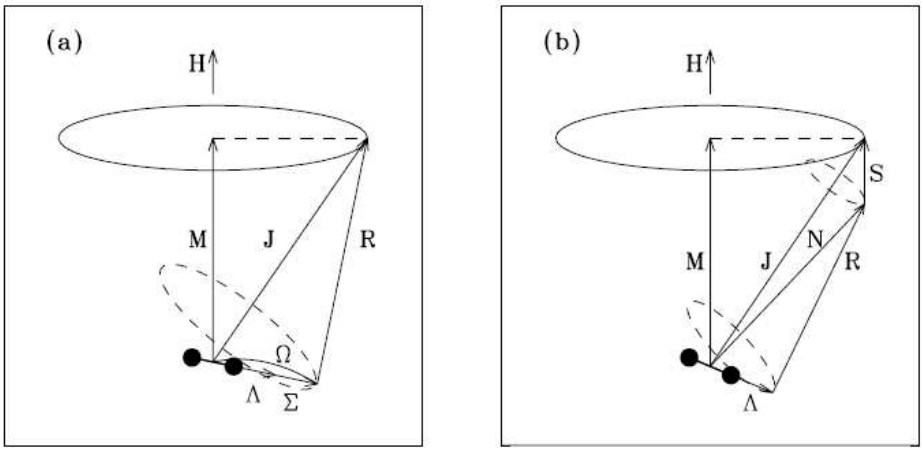

Figure 4.1: The meaning of molecular quantum numbers in the two Hund's cases (Berdyugina & Solanki, 2002).

Otherwise the notation is very similar to atomic notation

$$^{2S+1}\Lambda_{\Omega} \qquad \text{(molecule)} \tag{4.6}$$

$$^{2S+1}L_J \qquad \text{(atom)} \tag{4.7}$$

This is not quite enough to give a unique description for each electronic state of a molecule, so the spectroscopic term is preceded by a letter. This letter is X for the ground state, a capital letter (A, B, C, ...) for states with the same multiplicity (multiplicity is the value of 2S+1) than the ground state, and lower case letters (a, b, c, ...) for states with a different multiplicity than the ground state. In theory, the states are labelled in alphabetical order in ascending energy order, but for historical reasons this is not always the case. In comparison, for atoms the spectroscopic term is preceded by the principal quantum number.

Finally, the electronic energy E_e is the difference between minima of the two electronic potential curves involved in the transition. This difference is not easy to calculate because even a molecule as simple as C_2 contains two nuclei and 12 electrons.

A convenient way to describe the energy is to divide the energy by *hc*.

The values resulting from this are called term values. A similar treatment will be given to the vibrational and rotational energies as well (See below). The electronic term written in this way is

$$T_e = T_0 + A\Lambda\Sigma \tag{4.8}$$

where T_0 is the term value with neglected spin. A is a constant for a given term. The extra term rises from the fact that the internal magnetic field of the molecule causes the precession of $\overline{S}$ about the internuclear axis. The extra term causes the energy levels to split giving rise to the multiplicity of the molecular state. The value of A grows rapidly with increasing number of electrons.

4.1.2 Vibrational Energy

The electronic energy consideration mentioned in the previous section is similar for molecules and for atoms. But when more than one atom combines to form a molecule, other types of energies come into play. When there are two or more atoms together, the connections between the atoms are not infinitely rigid, so the molecule can vibrate.

The simplest approximation of a vibrating molecule is, naturally, a harmonic oscillator. This approximation leads to quantization

$$E_v = \hbar\sqrt{\frac{k}{\mu}}\left(v + \frac{1}{2}\right), \quad v = 0, 1, 2, 3, ... \tag{4.9}$$

The vibrational term is then E_v/hc and denoted by $\mathrm{G}(v)$.

$$G(v) = \frac{\hbar}{hc}\sqrt{\frac{k}{\mu}}\left(v + \frac{1}{2}\right) \tag{4.10}$$

$$G(v) = \omega\left(v + \frac{1}{2}\right) \tag{4.11}$$

Molecules are not ideal vibrators but close to the minimum of E_e the potential curve (See Figure 4.2) can be approximated as such using a series expansion and taking a suitable number of terms from the beginning. Thus,

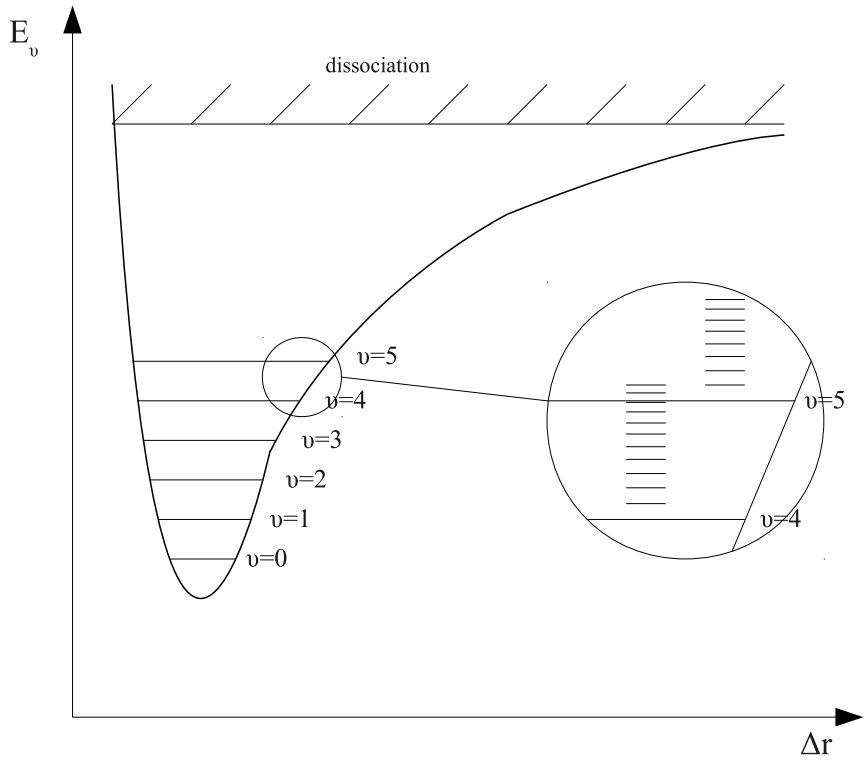

Figure 4.2: Energy level structure of one electronic state of a molecule. Each such state has several vibrational states (marked with v) and each of these, in turn, are composed of several rotational states (the inset figure).

for an anharmonic oscillator, the term value can be expressed as

$$G(v) = \omega_e \left(v + \frac{1}{2}\right) - \omega_e x_e \left(v + \frac{1}{2}\right)^2 + \omega_e y_e \left(v + \frac{1}{2}\right)^3 + ... \qquad (4.12)$$

where $\omega_e = \omega$(harmonic oscillator) and ω_e, $\omega_e x_e$, $\omega_e y_e$ are constants depending on the potential curve of the molecule.

4.1.3 Rotational Energy

The simplest model for a molecule rotation-wise is a dumbbell model where a solid rod has solid spheres at both ends. The energy of this kind of a system is

$$E_r = \frac{I\omega_r^2}{2} \tag{4.13}$$

where $I = \mu r^2$ is the moment of inertia of the molecule (μ is the reduced mass and r is the internuclear distance) and ω_r is the angular velocity. This can also be written as

$$E_r = \frac{P^2}{2I} \tag{4.14}$$

where $P = I\omega_r (= const)$ is the angular momentum of the molecule. The quantization of rotational energy works through the angular momentum:

$$\overline{P}^{\,2} = J(J+1)\hbar^2, \quad J = 0, 1, 2, 3, ... \tag{4.15}$$

where J is the total angular momentum quantum number of the molecule. The quantized energy is

$$E_r = \frac{\hbar^2}{2I} J(J+1) \tag{4.16}$$

and the rotational term is

$$F(J) = \frac{\hbar^2}{2Ihc} J(J+1) \tag{4.17}$$

$$F(J) = BJ(J+1). \tag{4.18}$$

As was the case with vibrational energy, the rigid rotator is too simple to describe a molecule. In a real molecule the internuclear distance can vary. In such a model the centrifugal force $F_c = \mu\omega^2 r_0$ is balanced by the restoring force of a "spring" $F = -k\Delta r$. This leads to the energy having two terms

$$E_r = \frac{\hbar^2}{2I_0} J(J+1) - \frac{\hbar^4}{2I_0^2 k r_0^2} J^2(J+1)^2 \tag{4.19}$$

and the corresponding rotational term can be written as

$$F(J) = BJ(J+1) - DJ^2(J+1)^2. \tag{4.20}$$

The second term is derived from the restoring force. It is worth to note that $B \ll D$.

The separation between consecutive lines can be calculated as

$$\Delta\nu = F(J+1) - F(J) = 2B(J+1) - D(J+1)^3. \tag{4.21}$$

This difference decreases with increasing J.

Finally, in a real molecule, vibration and rotation can occur at the same time. This leads to a vibrating rotator. The interaction between the two is neglected and the energy of the vibrating rotator is the sum of the vibrational energy of the anharmonic oscillator and the rotational energy of the nonrigid rotator. This leads to each vibrational level having rotational structure (See Figure 4.2). Also, the rotational constants B and D depend on the vibrational state and are denoted by B_v and D_v so that

$$F_v(J) = B_vJ(J+1) - D_vJ^2(J+1)^2. \tag{4.22}$$

In the term notation then

$$T = T_e + G_e(v) + F_v(J). \tag{4.23}$$

The frequency of a transition between two energy levels can be calculated as

$$\Delta\nu = T' - T'' = (T' - T'') + (G' - G'') + (F' - F'') \tag{4.24}$$

$$\Delta\nu = \nu_e + \nu_v + \nu_r. \tag{4.25}$$

Each vibrational state of the upper electronic state can combine with each vibrational state of the lower electronic state, which leads to a large number of vibrational transitions resulting in the formation of a band system.

The selection rule for molecular transitions is

$$\Delta J = (J' - J'') = 0, \pm 1, \tag{4.26}$$

if $\Lambda \neq 0$ for at least one of the two states and

$$\Delta J = \pm 1, \tag{4.27}$$

if $\Lambda = 0$ in both states (e.g. J=0 $\rightarrow$ 0 is not allowed). The different changes of J have been given names. They are the rotational branches:

$$R(J) = \nu_0 + F'_v(J+1) - F''_v(J) \qquad \Delta J = +1 \tag{4.28}$$
$$Q(J) = \nu_0 + F'_v(J) - F''_v(J) \qquad \Delta J = 0 \tag{4.29}$$
$$P(J) = \nu_0 + F'_v(J-1) - F''_v(J) \qquad \Delta J = -1 \tag{4.30}$$

The final phenomenon related to molecular spectra before magnetic fields are discussed is the so called band head of the vibrational transition. The locations of rotational lines in a given vibrational band follow the equation

$$\nu = \nu_0 + (B'_v + B''_v)m + (B'_v - B''_v)m^2 \tag{4.31}$$

where m=-J for P-branch and m=J+1 for R-branch. This function is a parabola and its effect on the spectral structure of a molecular band can be seen in Figure 4.3. The band heads are formed in different branches depending on the relative values of B_v in the upper and lower vibrational states of the transition. The band head forms in the blue end of the molecular absorption band in the case that $B'_v < B''_v$ and in the red end when $B'_v > B''_v$. In these cases the bands are said to be shaded towards red and blue, respectively, i.e. in the direction opposite the band heads.

4.2 Molecules in Magnetic Fields

The previous sections did not take the effects of magnetic fields into account in the treatment of the spectral structure of molecules. Magnetic fields have an effect on the structure of energy levels if the total magnetic moment of the molecule is non-zero. In such a case the external magnetic field interacts with the magnetic moment and makes the total angular momentum vector $\overline{J}$ precess about the field direction.

The space quantization of $\overline{J}$ results in 2J+1 magnetic components with

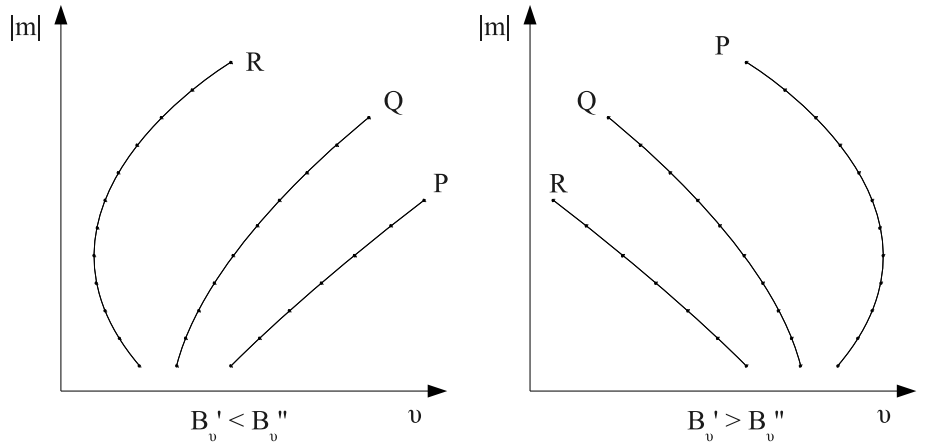

Figure 4.3: Schematic of how the location of a rotational line depends on the quantum number J and the relative strength of the rotational constants B_v in the upper and lower energy states of the transition.

different energies

$$\overline{J} = M\hbar, \quad M = J, J-1, J-2, ..., -J+1, -J. \tag{4.32}$$

The largest contributions to the magnetic momentum of a molecule come from the electronic spin, electronic angular momentum, momentum of nuclear rotation and nuclear spin, in descending order of importance. The energies of magnetic components and strengths of transitions depend on how the electronic momenta are coupled to the rotation of the molecule.

Two different cases exist for this coupling and they are named after their discoverer Hund's case a and b. Naturally, these cases represent the extremes and in some situations a treatment of an intermediate case is required.

In Hund's case a, also called strong coupling, the electronic spin and orbital angular momenta are strongly coupled to each other and only weakly interact with the nuclear rotation. In this case the multiplet splitting ($A\Lambda\Sigma$ in Equation 4.8) is larger than rotational splitting (Equation 4.21). If the interaction of the total angular momentum J with the external magnetic

field $\overline{H}$ (See the left panel of Figure 4.1) is much weaker than the interaction of $\Omega(=\Lambda+\Sigma)$ with the rotation, the Zeeman regime is appropriate and there is an additional splitting of energy levels according to

$$\Delta E = gM\mu_0 H, \quad g = \frac{\Omega(\Lambda+2\Sigma)}{J(J+1)} \tag{4.33}$$

where again M=J, J-1, J-2,..., -J+1, -J. Here, the Zeeman levels are equidistant. The splitting decreases rapidly as J increases. The selection rule for transitions in Hund's case a are:

$$\Delta\Lambda = 0, \pm 1 \tag{4.34}$$
$$\Delta\Sigma = 0 \tag{4.35}$$
$$\Delta J = 0, \pm 1 \tag{4.36}$$
$$\Delta M = 0, \pm 1 \tag{4.37}$$

with $J = 0 \to 0$ being forbidden as well as $\Delta J = 0$ when $\Omega = 0 \to 0$

In Hund's case b, also called weak spin coupling, the orbital angular momentum is coupled to the internuclear axis, but spin is only weakly coupled to the axis. If $\Lambda = 0$ and $S \neq 0$, spin is not coupled at all to the internuclear axis and quantum numbers $\overline{\Sigma}$ and $\overline{\Omega}$ are not defined. In Hund's case b the orbital angular momentum $\overline{\Lambda}$ and the angular momentum of nuclear rotation $\overline{R}$ form a moment $\overline{N}$ (See the right panel of Figure 4.1)

$$\overline{N} = \overline{\Lambda} + \overline{R} \tag{4.38}$$
$$N = \Lambda, \Lambda+1, \Lambda+2, ..., \Lambda+R \tag{4.39}$$

Now $\overline{N}$ and $\overline{S}$ together form the total angular momentum $\overline{J}$ of the molecule.

$$\overline{J} = \overline{N} + \overline{S} \tag{4.40}$$
$$J = N+S, N+S-1, ..., |N-S| \tag{4.41}$$

This way each rotational level splits into 2S+1 multiplet components. For Hund's case b the rotational splitting is larger than the multiplet splitting

and selection rules for allowed transitions are as follows:

$$\Delta J = 0, \pm 1 \tag{4.42}$$

$$\Delta N = 0, \pm 1 \tag{4.43}$$

$$\Delta S = 0 \tag{4.44}$$

with $J = 0 \to 0$ forbidden again. Also for transitions for which $\Lambda = 0 \to 0$, $\Delta K \neq 0$ where K is the projection of N on the internuclear axis. If $\Delta J = \Delta N$ we get the main branches (R,Q,P) and if $\Delta J \neq \Delta N$ we get so called satellite branches.

Zeeman splitting in Hund's case b takes the form

$$\Delta E = \mu_0 M H g \tag{4.45}$$

where

$$g = \frac{1}{J(J+1)} \left\{ \frac{\Lambda^2}{2N(N+1)} [J(J+1) + N(N+1) - S(S+1)] + \right.$$
$$\left. + J(J+1) - N(N+1) + S(S+1) \right\} \tag{4.46}$$

is the Landé g-factor. The Zeeman levels are equidistant in energy and there are 2J+1 of them for each J.

Sometimes the coupling between $\overline{N}$ and $\overline{S}$ is so weak that even a small field can uncouple them. In this case the magnetic splitting happens through the Paschen–Back effect. Now $\overline{N}$ and $\overline{S}$ are quantized independently of each other and the resulting split of energy levels becomes

$$\Delta E = \left(\frac{\Lambda^2}{N(N+1)} M_N + 2M_S \right) \mu_0 H \tag{4.47}$$

$$= g_N M_N \mu_0 H + g_S M_S \mu_0 H \tag{4.48}$$

This is valid as long as the multiplet splitting is small compared to Zeeman splitting.

4.3 Carbon molecules in DQ White Dwarfs

In DQ white dwarfs the molecule responsible for the absorption features in the optical wavelengths is C_2. In only two WDs (G99-37 and GJ841B) there are traces of CH. C_2 has many transitions (Cooper & Nicholls, 1975) which have been studied already decades ago in the laboratory. The electronic transitions of interest to astronomy are the ones that can be seen in the optical wavelength region. These have been named Swan bands and Deslanders-d'Azambuja bands. The former includes all the vibrational and rotational transitions of the electronic transition $d^3\Pi_g - a^3\Pi_u$ and the latter $C^1\Pi_g - A^1\Pi_u$, both for the molecule C_2. In two DQ WDs absorption bands of the molecule CH are also visible. There are two of these bands, $A^2\Delta - X^2\Pi$ and $B^2\Sigma - X^2\Pi$, in the optical.

The Swan bands with vibrational transitions $\Delta v = 2, 1, 0, -1$ have bandheads approximately at wavelengths 437 nm, 475 nm, 517 nm and 563 nm, respectively. Their strengths varies from object to object depending on temperature and carbon abundance, but they are the most clearly visible carbon features in both cool and peculiar DQ WDs.

The Deslanders-d'Azambuja bands with vibrational transitions $\Delta v = 2, 1, 0, -1$ have bandheads between 340 nm and 420 nm. Due to the poor sensitivity of CCDs in the blue end of the spectrum and the intrinsic faintness of the bands, these bands are rarely clearly seen in the spectra of DQ WDs. In the magnetic G99-37 these bands can be seen blended together with the CH bands (Berdyugina, Berdyugin & Piirola, 2007).

The two CH electronic transitions form absorption bands at wavelengths at 386 nm and 430 nm. In these all the vibrational transitions are overlapping, which also explains the strong polarization signals present in these bands (Berdyugina, Berdyugin & Piirola, 2007; Vornanen et al., 2010). The effect of magnetic field is summed from each vibrational band and so the combined polarization can reach very high levels.

The Swan bands can be used as an example of what the symbols in the electronic transition mean. The two terms are the spectroscopic notations of the lower and upper energy states, respectively. Π means that the orbital angular momentum is 1 in both of them. The superscript 3 means that $S = 1$ ($2S + 1 = 3$) for both states. The first letter in both terms is the equivalent of the atomic principal quantum number, which tells on which electronic energy level the states are. The letters are lower case because the multiplicity ($2S+1 = 3$) of the ground state is not 3. Level a is the first level

above the ground state and d is the fourth level. The small subscript letter in the end tells the parity of the molecule. These have not been discussed before. The letter g stands for gerade (even in German) and u for ungerade (odd in German). The parity has to change in electronic dipole transitions, which are the most common transitions in molecules. The parity is related to the behaviour of the molecule's wavefunction with respect to a reflection at the center of symmetry.

The rotational excitation of a molecule is not evident from the notation of molecular transitions. In Paper I values of the total angular momentum quantum number J go up to 70. In the modelling presented in Section 4.4 J values are as high as 150. Also, the temperature sensitivity of the model increases when additional rotational levels are taken into account. This leads to a more accurate temperature determination based on the shape of the molecular absorption bands, but only if the observations are accurate enough to show the very small differences. Additional inaccuracies arise from the linelists for molecules. Extrapolation is used to get the transition energies for higher values of J and errors in the extrapolation increase with increasing J.

When all the energy levels of electronic, vibrational and rotational states are known and they are split according to the possibly present external magnetic field, the allowed transitions between levels can be calculated taking into account all selection rules. When all the possible lines are known, each line is given some depth and width according to physical conditions in the WD. When the shape of each line is known and their effects summed for each wavelength, the Stokes parameters at each wavelength have finally been obtained.

In the model used in this thesis each line is given some depth based on the strengths of the Zeeman components of the transition and its oscillator strength. Temperature also affects the line depth as well as radiative dampening. There is also a free parameter that adjusts the depth of all lines in an absorption band. Line width is controlled by a single parameter and it is used to match the model to the instrumental broadening in the observations. One way to do the required calculations is described in Appendix A where the Unno-Rachkowsky solution of polarized radiative transfer in a Milne-Eddington atmosphere is presented. This model was used in Paper I to model the Swan bands of GJ841B.

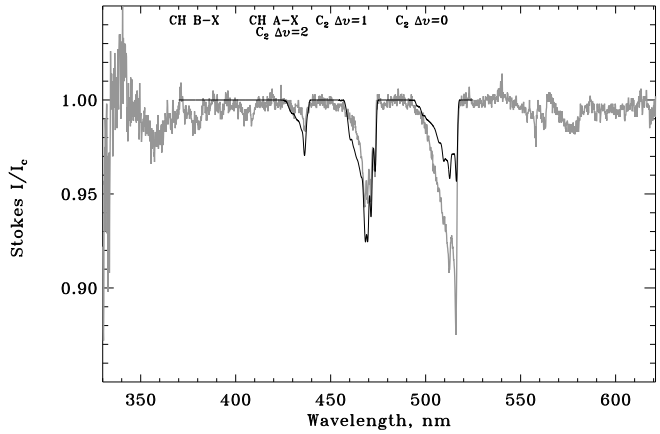

Figure 4.4: Best fitting model for GJ893.1 using the model from Berdyugina, Berdyugin & Piirola (2007) with a temperature of 7000K.

4.4 Modelling issues

For the papers included in this thesis, I have tried to model the Swan bands of C_2 to get the physical conditions where the molecules are in the WD atmospheres. Unfortunately some difficulties arose and the model of Berdyugina, Berdyugin & Piirola (2007) did not reproduce the observed features as expected.

To illustrate the problems of modelling the intensity features Figure 4.4 shows a best fit we could originally find for GJ893.1 using the model from Berdyugina, Berdyugin & Piirola (2007). The model has a temperature of 7000 K close to the value (7440 K) found by Dufour, Bergeron & Fontaine (2005). The mismatch of the depth of the differenct bands ($\triangle v = 2, 1, 0$) is clearly visible.

The temperature based on the molecules does not have to be same as the photospheric temperature usually reported for white dwarfs (like the 7440 K for GJ893.1 mentioned above). Instead, the temperature where the molecules are can be as low as a few thousand kelvins. This lower temperature actually has the effect of changing the relative depths of the absorption bands to match more closely the observed ratios. In Figure 4.5 the temperature is 2000 K and the ratio of $\triangle v = 1$ to $\triangle v = 0$ is closer to

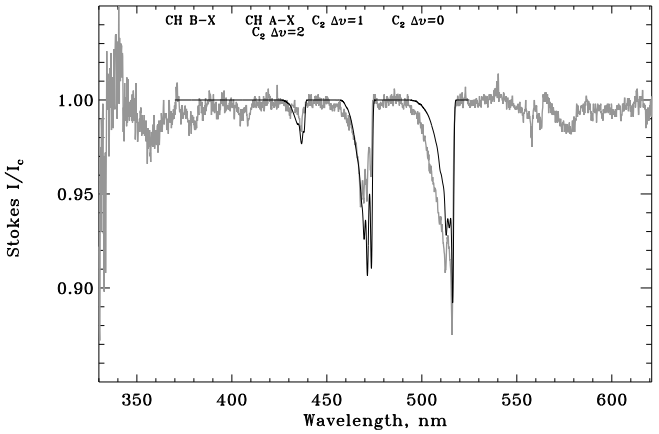

Figure 4.5: Model for GJ893.1 with a temperature of 2000 K.

the observed ratio. However, if the temperature is dropped even further the shapes of the bands start to change and the fit gets worse, even if the ratio of band depths would be better.

The model can be used to construct some more complex atmospheric structures by combining model calculations with different parameters in certain ways. I have to note that these are mere toy models and are no substitute for an actual 3D atmospheric model.

First, I tried to model the atmosphere using two components in a manner of a spot and an atmosphere. Two spectra were combined in the following way:

$$Spectrum = f \cdot Spectrum1 + (1 - f) \cdot Spectrum2 \qquad (4.49)$$

where f is a filling factor of the spot (how large a fraction it covers from the atmosphere) and Spectrum1 and Spectrum2 are the spectra of the models used as the spot and atmosphere, respectively.

After running all possible combinations of models in our grid and different spot sizes, the best possible solution turned out to be not much better than the original (See Figure 4.6) The model has a spot of 6000 K covering 10 % of the atmosphere in an atmosphere of 8000 K. A spot like this would cause the brightness of the star to vary as the spot moves across the visible

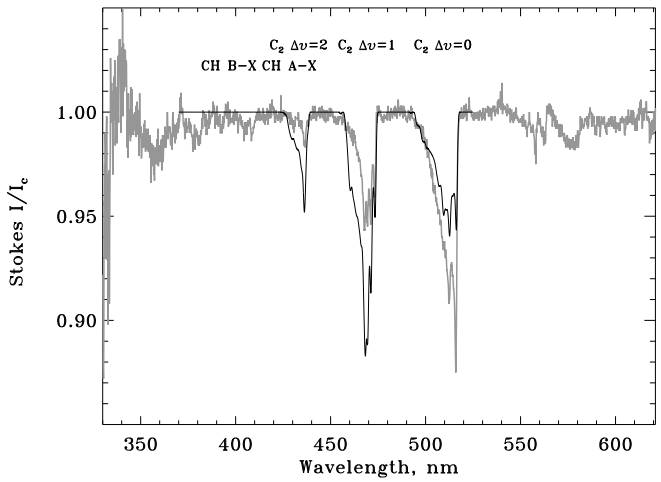

Figure 4.6: Best fitting model for GJ893.1 using the model from Berdyugina, Berdyugin & Piirola (2007) with a spot of 6000 K in an atmosphere of 8000 K. Spot covers 10 % of the visible hemisphere.

hemisphere. I tried to observe such photometric changes, but I was not succesful. See Paper II for details.

Next, I added a third component to the atmosphere and used the components as stratified layers in the WD atmosphere. Just like in the spot modelling scenario, I used the simplest possible way of adding the effect of several layers of absorbing atmosphere. I did this by multiplying the spectra of the layers by one another to get the combined absorption from a stratified atmosphere. This does not take into account emission from each layer, however, but it still works as a first approximation.

Again we tried to find the best solution by least squares fitting using all possible combinations of our models and the best possible fit is shown in Figure 4.7. The fit is much better than with the spot model, but still far from adequate. The temperatures for the different layers are very low (two layers with temperatures 2000 K and 2500 K in this case) but the molecules can very well be at a different altitude than the photosphere, which has a temperature usually between 6000 K and 9000 K.

I also tried to increase the maximum of the total angular momentum

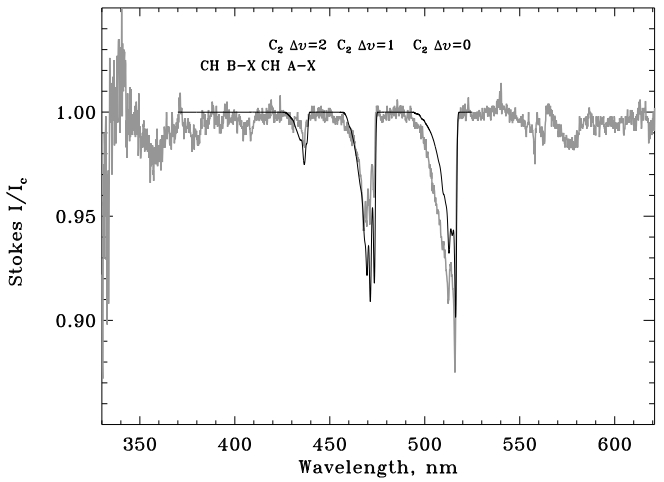

Figure 4.7: Best fitting model for GJ893.1 using the model from Berdyugina, Berdyugin & Piirola (2007) with a stratified atmosphere.

J. By increasing it to 150 from the original 70 especially the blue wings of the absorption bands get stronger, but it also changes the shape of the absorption features a little. Because the added number of lines meant increased calculation times, the code was modified to calculate only Stokes I and use $B = 0$ G. At the same time the $\triangle v = -1$ band was added to the model. The original problem persisted, however. Figure 4.8 shows a model similar to 4.5, but with the increased J. Adding more lines shows as increased absorption as well as changing the shape of the bands slightly.

Because we exhausted our options of using physically logical models to fit the data, we tried to see what would it take to get models fit. There are two parameters in the model that control the depth of individual absorption lines within the wide bands. The first one are the oscillator strengths of C_2. They tell us how deep an absorption line we get from a transition between certain energy levels of the molecule. By adjusting these values it is possible to get a very good fit as shown in Figure 4.9. These values are determined in a laboratory, and while they have error limits, we had to modify the values by several orders of magnitude to get a good fit and that is not plausible.

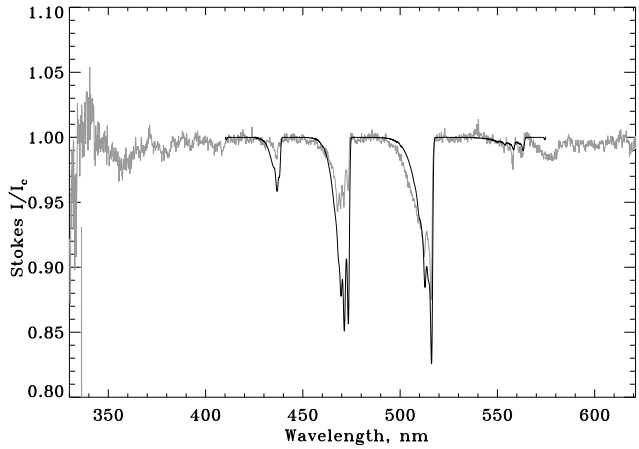

Figure 4.8: Same as Figure 4.5, but with J increased from 70 to 150 and $\triangle v = -1$ added.

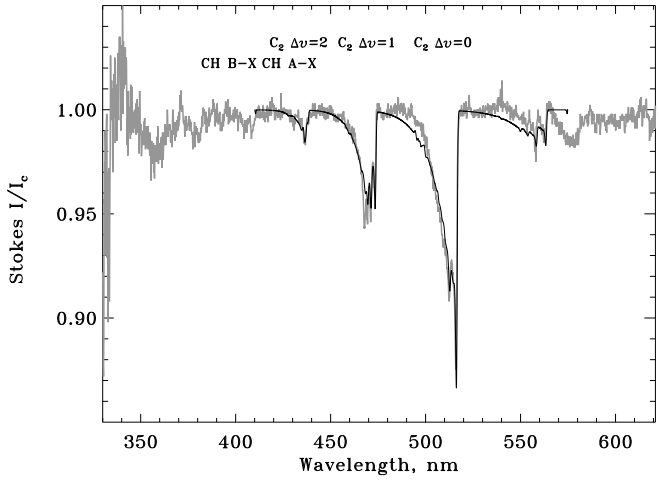

Figure 4.9: A good fit achieved by changing the oscillator strengths of C_2.

Finally, there is a parameter in the model that controls the depth of each line in an absorption band. In the models above, the parameter was kept the same for all bands, but it can be adjusted individually for each band. However, there is no apparent connection between this parameter and a physical parameter, so we thought it wise not to play around with it in this way. This parameter should be connected with carbon abundance in the atmosphere, since they have the same effect on the absorption bands.

In conclusion, the method in Berdyugina, Berdyugin & Piirola (2007) can be used to model the C_2 features on cool DQ white dwarfs, but the method is not yet fully operational and more work needs to be done to make it a useful tool in white dwarf research.

The method, once perfected, can be used to study other stars as well. There are, for example, giant stars with C_2 in their atmospheres as well as other diatomic molecules, for which the same method can be used (Green, 2013).

Chapter 5

Conclusions

To put all our information about DQ white dwarfs together, we can say that there indeed seems to be two sequences of DQs (Dufour et al., 2008). The hot DQs have very high carbon abundances and a high incidence of magnetism. The cool DQs (warm, cool and peculiar put together) have a smaller incidence of magnetism ($\approx 4\%$) and there is large variation in the abundance of carbon as evidenced by the large variation in Swan band depths among the objects in Paper III.

To confirm the existence of these two sequences modelling of high carbon abundance in lower temperatures should be done. WD1235+422 mentioned in Paper III is a good candidate for a cool DQ with a high carbon abundance, for example. There should be similar objects among the warm DQs as well, but modelling is needed to figure out what their spectra should look like.

The sample of DQ WDs is very small compared to DA and DB white dwarfs. Future surveys will undoubtedly increase the sample size and also extend the sky coverage of known stars. Currently most of the DQs are from the Sloan Digital Sky Survey (SDSS) and are thus limited to a portion of the northern hemisphere close to the ecliptic. This creates problems because many of the largest European telescopes are in Chile. Also, the lack of spectropolarimetric capabilities in the largest telescopes is a major hindrance for detecting and quantifying magnetic fields. The planned extremely large telescopes will also solve the problem that most DQs are very faint, provided that their instumentation is suitable for WD research.

The modelling method used in this thesis shows promise of being a useful diagnostic tool for molecular spectropolarimetry but, as always, more work needs to be done to perfect it.

Chapter 6

Summary of Papers

6.1 Observations For This Thesis

For this thesis I have observed 12 white dwarfs for the first time with spectropolarimetry. Observations of one additional WD are also included in this thesis. This WD was observed by a colleague as a backup target during a non-related observing programme. Two WDs were also observed photometrically in B and R bands.

The spectropolarimetric observations were done with three different telescopes: The Nordic Optical Telescope (NOT) and the Unit Telescopes 1 (for the one additional WD) and 2 on the Very Large Telescope (VLT). At the NOT the ALFOSC instrument was used, which is a multi-purpose instrument capable of photo(polari)metry and spectro(polari)metry in the optical wavelength region. At the VLT telescopes the instruments FORS 1 and 2 were used. They are similar to ALFOSC but only FORS1 on the UT2 had polarization capabilities. After decommissioning of FORS1 the polarization optics were transferred to FORS2 on the UT1.

In the FORS observations grism 600B+12 was used, which gives a resolution of R =780, or 0.5 nm at 400 nm. NOT is much smaller than VLT so something has to compensate for the smaller size to get a good signal to noise ratio. For that reason a very low resolution grism #10 and a wide slit (1.8") were used. Together they allow for a spectral resolution as low as 70. This means 5.7 nm at 400 nm. This is a very low resolution, but then again, the molecular features are dozens of nanometers wide so it was possible to detect possible polarization signals just as well with this lower resolution.

First of our observing runs was with the VLT and FORS1 instrument in 2008. We observed 6 DQ WDs including G99-37 which was already known

to be magnetic. One object, GJ893.1 was observed with FORS2 in 2009 (at this time the polarization optics had been transferred from FORS1) as a backup target in another observing program. NOT observations were done in 2010 when we observed another 6 DQ WDs as well as G99-37. Follow up observations of WD1235+422 were done in service mode with the NOT on two occasions: May 2011 and March 2013.

Photometric observations were done during the spring of 2011 with the KVA (Kungliga Vetenskapsakademien) telescope situated on La Palma in the Canary Islands. This telescope is actually two telescopes in one. The main telescope has 60 cm main mirror and attached to the support structure of the telescope is a 35 cm Schmidt-Cassegrain Celestron telescope. The bigger telescope is used for photopolarimetry and the smaller one for photometry. The telescopes are controlled remotely by researchers at Tuorla observatory who use them mostly for monitoring the optical brightness of targets of the MAGIC telescopes. Another project that uses the telescopes is the study of interstellar polarization in the solar neighborhood.

6.2 Paper I

In this paper I reported on the most important discovery from our survey of cool DQ white dwarfs, which was made from our first observing run with VLT in 2008. I discovered the second cool DQ WD showing a polarized absorption feature of CH in its spectrum. The first such star (G99-37) was discovered in 1974 (Angel & Landstreet, 1974). GJ841B has a polarized CH feature just like G99-37, but the feature is a little weaker both in intensity and in circular polarization. GJ841B is also the first star in this class to show polarized C_2 features. Polarization in these features is quite weak and we can't rule out the possibility that the signal is due to noise. The flux is much weaker in the absorption bands, which in turn leads to a weaker S/N in the Stokes V/I spectra.

Modelling of GJ841B using a simple homogeneous magnetic field and a pole-on view produced a surface temperature of 6100 K and a magnetic field strength of 1.3 MG. These values are very close to the values of G99-37 (6200 K and 7.3 MG) gotten from the same observing run. This means that the stars are very similar, although there are differences as well. The CH feature is weaker in intensity in GJ841B but the C_2 absorption bands are much stronger. The circular polarization visible in the C_2 Swan bands in

GJ841B could be a result of the larger amount of C_2. I also found small amounts of linear polarization in GJ841B, which could indicate a non-pole-on viewing geometry, but the signal is weak and could be just due to weaker signal in the absorption bands.

More complex field and viewing geometries should be tested but that will take some code development and additional modelling, which are beyond the scope of this study.

6.3 Paper II

In this paper I reported on our photometric campaign to monitor two of the DQ WDs from our spectropolarimetric survey. I could not fit the C_2 Swan bands of any of our WDs properly with the original code and one possible solution to this problem was to combine two models in the manner of a spot and a surrounding atmosphere. This gave better fits to the intensity spectra. This hypothesis could be tested with photometric observations because the spot would cause brightness variations as it moves across the visible hemisphere of the star.

Analysis of the lightcurves did not, however, reveal any variability for these stars. With perfect hindsight, I calculated probabilities of missing spots and they were quite high for both of the WDs. The chances of missing a spot of size 10 % of the visible hemisphere was 81 % for EGGR78 and 68 % for GJ1117 leading to a 55 % chance of missing a spot on both stars. In other words, we had only a 45 % chance of detecting a spot on at least one of the stars. Missing a spot in this case means that the brightness variability caused by it moving across the visible hemisphere is smaller than the sensitivity of the observations.

Reason for this low chance of detection was the small changes that a spot would have on the spectra. And our choice of using the B band was clearly wrong. The sensitivity curve of B band is only sensitive to the shallow $\Delta v = 2$ Swan band. In retrospect, V band would have been a better choice, because it includes both the $\Delta v = 1$ and $\Delta v = 0$ bands, which are much more pronounced than the $\Delta v = 2$ band. Also the two WDs we observed, EGGR78 and GJ1117, were quite poor choices. EGGR78 has extremely weak Swan bands so detecting changes in them is almost impossible. GJ1117 has stronger bands but they are obscured by atomic lines of carbon. These stars were selected based on suitable right ascensions

and declinations, and they were the only suitable ones.

6.4 Paper III

In this paper I reported our findings from the survey of cool DQ white dwarfs. Apart from GJ841B reported in Paper I, I found polarization in only one of the 12 WDs that were studied with spectropolarimetry for the first time. WD1235+422 has very strong absorption features of C_2 that are starting to blend to each other. The star also shows a strong polarization signal across the optical wavelength region. The polarization behaviour reminds those of peculiar DQs and the intensity features as well are similar to those in peculiar DQs although to a lesser extent. This object seems to be intermediate between normal cool DQs and peculiar DQs and as such a very interesting star for further studies. Our observations do not have a sufficient S/N for accurate modelling and the model also needs some upgrades to handle more extreme conditions to work on WD1235+422, but this star definitely warrants further research.

Original intention was to show modelling of intensity features of C_2 Swan bands and based on those and lack of circular polarization give atmospheric parameters and upper limits of magnetic field strength for the stars. But during the modelling effort I noticed that there was no way of getting reasonable results and in the end we had to leave them out of the paper. The model does not take the WD atmosphere into account in sufficient detail to be useful so we had to settle for just reporting observational results.

Appendix A

Radiative Transfer

This Appendix includes a rather long list of equations needed to get the full Stokes vector of a observations of a magnetic source. The physical problem they address is, how does polarized radiation move through a medium. The solution to this problem is the so-called Unno-Rachkowsky solution (Unno, 1956; Rachkovsky, 1962a,b) of radiative transfer. The papers by Rachkovsky are written in Russian and are hard to find, but fortunately the method is described in detail also in Landi Degl'Innocenti (1976). The solution gives the Stokes parameters as described below. Model for the stellar atmosphere used in this study is a Milne-Eddington atmosphere, which is a plane-parallel model, i.e. the atmosphere is described as a slab of material where its properties only vary with depth or remain constant (like the magnetic field). A true stellar atmosphere is a layer on a sphere and properties in it change with horizontal location as well as the vertical and magnetic fields in white dwarfs usually have a dipole configuration, but the approximation still gives usable predictions. The derivation of the equations presented here can be found in Stenflo (1994).

The coordinate system used in these equations is presented in Figure A.1 where $\mathbf{e}_\alpha$ is the unit vector of linear polarization that has a length of 1 and whose direction tells the direction of linear polarization.

The end result of radiative transfer is the Stokes vector that we can observe (assuming interstellar space and Earth's atmosphere do not have

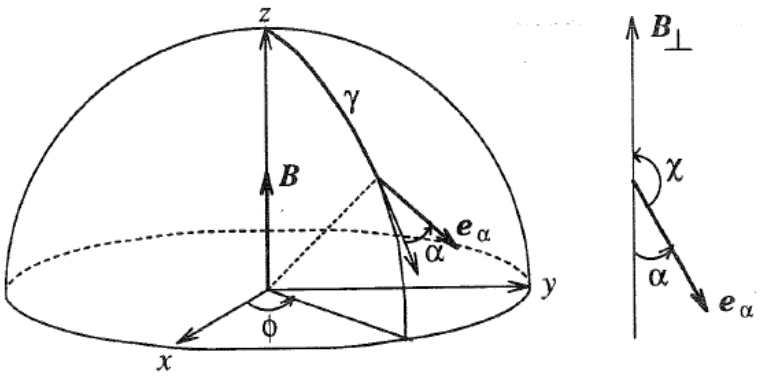

Figure A.1: Coordinate system used in the derivation of radiative transfer equations. $\mathbf{B}$ is the magnetic field vector, $\mathbf{B}_\perp$ its projection on a plane perpendicular to the propagation direction. γ is the angle between the beam and the magnetic field, χ the angle of $\mathbf{B}_\perp$ with respect to the polarization vector $\mathbf{e}_\alpha$.

an effect).

$$I/I_c = 1 + \beta + \beta(\eta_I + 1)[(\eta_I + 1)^2 + d]/\Delta \tag{A.1}$$

$$Q/I_c = -\beta[(\eta_I + 1)^2\eta_Q + (\eta_I + 1)(\rho_U\eta_V - \rho_V\eta_U) + s\rho_Q]/\Delta \tag{A.2}$$

$$U/I_c = -\beta[(\eta_I + 1)^2\eta_U + (\eta_I + 1)(\rho_V\eta_Q - \rho_Q\eta_V) + s\rho_U]/\Delta \tag{A.3}$$

$$V/I_c = -\beta[(\eta_I + 1)^2\eta_V + (\eta_I + 1)(\rho_Q\eta_U - \rho_U\eta_Q) + s\rho_V]/\Delta \tag{A.4}$$

where

$$\Delta = (\eta_I + 1)^2[(\eta_I + 1)^2 - a + d] - s^2 \tag{A.5}$$

$$a = \eta_Q^2 + \eta_U^2 + \eta_V^2 \tag{A.6}$$

$$d = \rho_Q^2 + \rho_U^2 + \rho_V^2 \tag{A.7}$$

$$s = \eta_Q\rho_Q + \eta_U\rho_U + \eta_QV\rho_V \tag{A.8}$$

$$\beta = \frac{\beta_0\mu}{1 + \beta_0\mu}. \tag{A.9}$$

In the last equation $\mu = \cos\theta$ where θ is the angle between the line of sight and the z-axis (direction of the magnetic field). β in the last equation is the so called limb-darkening factor which derives from the depth dependence of the Planck function:

$$B_\upsilon(\tau) = B_0(1 + \beta_0\tau) \tag{A.10}$$

where a simple linear dependence of the blackbody emission (B_υ) on the optical depth (τ) is assumed.

The η's and ρ's in the above equations are the elements of the line absorption matrix

$$\boldsymbol{\eta} = \begin{pmatrix} \eta_I & \eta_Q & \eta_U & \eta_V \\ \eta_Q & \eta_I & \rho_V & -\rho_U \\ \eta_U & -\rho_V & \eta_I & \rho_Q \\ \eta_V & \rho_U & -\rho_Q & \eta_I \end{pmatrix} \tag{A.11}$$

and have the forms

$$\eta_{I,Q,U,V} = \eta_0 H_{I,Q,U,V} \tag{A.12}$$

$$\rho_{Q,U,V} = 2\eta_0 F_{Q,U,V} \tag{A.13}$$

where $\eta_{I,Q,U,V}$ are absorption coefficients and $\rho_{Q,U,V}$ are dispersion coefficients related to magneto-optical effects. The simple equations above are the result of using a Milne-Eddington atmosphere, which is an idealization making the assumption that the absorption matrix in Equation A.11 is depth independent. This carries with it also the idea that the magnetic field is homogeneous, which it is not. The previous equations include a coefficient η_0

$$\eta_0 = \kappa_0/\kappa_c \tag{A.14}$$

where κ_0 is the coefficient of absorption at the line center and κ_c the coefficient of continuous absorption. The H terms contain the effects of absorption and the F terms the effects of anomalous dispersion, also called

the magneto-optical effects:

$$H_I = H_\Delta \sin^2\gamma + \frac{1}{2}(H_+ + H_-) \tag{A.15}$$

$$H_Q = H_\Delta \sin^2\gamma \cos 2\chi \tag{A.16}$$

$$H_U = H_\Delta \sin^2\gamma \sin 2\chi \tag{A.17}$$

$$H_V = \frac{1}{2}(H_+ + H_-)\cos\gamma \tag{A.18}$$

where

$$H_q = H(a, \upsilon - q\upsilon_H), \quad q = 0, \pm 1 \tag{A.19}$$

$$H_\Delta = \frac{1}{2}[H_0 - \frac{1}{2}(H_+ + H_-)]. \tag{A.20}$$

In these equations γ is the angle between the polarization vector and the projection of $B_\perp$ on a plane perpendicular to the propagation direction and χ is the angle between the beam and the magnetic field. Parameter a is a damping parameter and has an expression $a = \frac{\mu_0 e^2 \omega^2}{12\pi mc\Delta\omega}$. Similar expressions for $F_{I,Q,U,V}$ are obtained by replacing H with F.

The $H(a, \upsilon - q\upsilon_H)$ and $F(a, \upsilon - q\upsilon_H)$ are given by equations

$$H(a, \upsilon) = \frac{a}{\pi}\int_{-\infty}^{+\infty} \frac{e^{-y^2}dy}{(\upsilon - y)^2 + a^2} \tag{A.21}$$

$$F(a, \upsilon) = \frac{1}{2\pi}\int_{-\infty}^{+\infty} \frac{(\upsilon - y)e^{-y^2}dy}{(\upsilon - y)^2 + a^2} \tag{A.22}$$

where $H(a, \upsilon)$ is the Voigt function and $F(a, \upsilon)$ is the line dispersion function. Note that H integrated over υ gives $\sqrt{\pi}$ to make $H(0, 0) = 1$.

Earlier, in Equation A.14, there were two coefficients of absorption; the coefficient of absorption at the line center κ_0 and κ_c the coefficient of continuous absorption. The first one has the following form:

$$\kappa_0 = \frac{2\omega k_N}{\sqrt{\pi}c} \tag{A.23}$$

where k_N is the normalization factor of a refractive index n_q induced by the vector component q of the vibrations of the EM vector (The polarization vector $\mathbf{e}_\alpha$ in Figure A.1 is transformed into spherical coordinates, which are

denoted by q=0,±1.) and given by

$$k_N = \frac{\pi\omega_A^2}{4\omega_0\Delta\omega_D}. \tag{A.24}$$

$\Delta\omega_D$ is a frequency width used to normalize all frequencies and chosen to be the Doppler width and

$$\omega_A = \sqrt{\frac{e^2N}{\epsilon_0 m}} \tag{A.25}$$

where ω_A is the frequency parameter for classical oscillators. It would be equal to the plasma frequency if N were equal to N_e, the electron number density. In this case N is the number density of classical oscillators. Alternatively k_N can be given in form

$$k_N = \frac{e^2Nf}{16\pi\nu_0\Delta\nu_D} \tag{A.26}$$

where f is the oscillator strength and the angular frequency $\Delta\omega_D$ has been replaced by the frequency $\Delta\nu_D$ ($\nu = \omega/2\pi$) and $\Delta\nu_D$ is the Doppler broadening of a spectral line. The code used for modeling in this thesis uses this form of k_N.

To make a connection with measurable quantities, υ in Equation A.19 needs to be given as a function of some physical quantities. The parameter υ_q is defined as

$$\upsilon_q = \upsilon - q\upsilon_H \tag{A.27}$$

where

$$\upsilon = (\nu_0 - \nu)/\Delta\nu_D \tag{A.28}$$

$$q\upsilon_H = \Delta\nu_H/\Delta\nu_D \tag{A.29}$$

where ν_0 is the frequency of the line center and $\Delta\nu_H = \Delta\omega_H/(2\pi)$ is the Zeeman splitting given by

$$\Delta\omega_H = (g_l M_l - g_u M_u)\omega_L \tag{A.30}$$

where g_l and g_u are the Landé factors of the lower and upper level in tran-

sition and M_l and M_u are the corresponding magnetic quantum numbers. υ_q is also given by

$$\upsilon_q = (\omega_0 - \omega - q\omega_L)/\Delta\omega_D \tag{A.31}$$

where ω_L is the Larmor frequency known from plasma physics

$$\omega_L = \frac{e}{2m}B. \tag{A.32}$$

With these equations and the physical properties of the WD atmosphere, the polarization and intensity profiles of a WD can be calculated. In the case of DQ WDs, the amount of lines is truly huge and the calculations take a long time.

Bibliography

Angel J. R. P., Landstreet J. D., 1974, ApJ, 191, 457

Appenzeller I. et al., 1998, The Messenger, 94, 1

Bagnulo S., Landolfi M., Landstreet J. D., Landi Degl'Innocenti E., Fossati L., Sterzik M., 2009, PASP, 121, 993

Bagnulo S., Landstreet J. D., Fossati L., Kochukhov O., 2012, A&A, 538, A129

Barlow B. N., Dunlap B. H., Rosen R., Clemens J. C., 2008, ApJ, 688, L95

Berdyugina S. V., Berdyugin A. V., Piirola V., 2007, Physical Review Letters, 99, 091101

Berdyugina S. V., Solanki S. K., 2002, A&A, 385, 701

Bradt H., 2008, Astrophysics Processes

Brinkworth C. S., Marsh T. R., Morales-Rueda L., Maxted P. F. L., Burleigh M. R., Good S. A., 2005, MNRAS, 357, 333

Cooper D. M., Nicholls R. W., 1975, J. Quant. Spec. Radiat. Transf., 15, 139

del Toro Iniesta J. C., 2003, Introduction to Spectropolarimetry, del Toro Iniesta, J. C., ed.

Donati J.-F., Landstreet J. D., 2009, ARA&A, 47, 333

Dufour P., Bergeron P., Fontaine G., 2005, ApJ, 627, 404

Dufour P., Fontaine G., Bergeron P., Béland S., Chayer P., Williams K. A., Liebert J., 2010, in American Institute of Physics Conference Series, Vol. 1273, American Institute of Physics Conference Series, K. Werner & T. Rauch, ed., pp. 64–69

Dufour P., Fontaine G., Liebert J., Schmidt G. D., Behara N., 2008, ApJ, 683, 978

Dufour P., Liebert J., Fontaine G., Behara N., 2007, Nature, 450, 522

Fontaine G., Wesemael F., 1987, in IAU Colloq. 95: Second Conference on Faint Blue Stars, A. G. D. Philip, D. S. Hayes, & J. W. Liebert, ed., pp. 319–326

Green E. M., Dufour P., Fontaine G., Brassard P., 2009, ApJ, 702, 1593

Green P., 2013, ApJ, 765, 12

Hall P. B., Maxwell A. J., 2008, ApJ, 678, 1292

Hartquist T. W., 1990, Molecular Astrophysics, Hartquist, T. W., ed.

Herwig F., 2005, ARA&A, 43, 435

Iben, Jr. I., 1984, ApJ, 277, 333

Iben, Jr. I., 1991, ApJS, 76, 55

Kawaler S. D., Novikov I., Srinivasan G., eds., 1997, Stellar remnants

Kemp J. C., Swedlund J. B., Landstreet J. D., Angel J. R. P., 1970, ApJ, 161, L77

Koester D., Girven J., Gänsicke B. T., Dufour P., 2011, A&A, 530, A114+

Külebi B., Jordan S., Euchner F., Gänsicke B. T., Hirsch H., 2009, A&A, 506, 1341

Landi Degl'Innocenti E., 1976, A&AS, 25, 379

Landi Degl'Innocenti E., Landolfi M., eds., 2004, Astrophysics and Space Science Library, Vol. 307, Polarization in Spectral Lines

Landolt A. U., 1968, ApJ, 153, 151

Liebert J., Bergeron P., Eisenstein D., Harris H. C., Kleinman S. J., Nitta A., Krzesinski J., 2004, ApJ, 606, L147

Liebert J., Bergeron P., Holberg J. B., 2003, AJ, 125, 348

Montgomery M. H., Williams K. A., Winget D. E., Dufour P., De Gennaro S., Liebert J., 2008, ApJ, 678, L51

Piirola V., Vornanen T., Berdyugin A., Coyne, G. V. S. J., 2008, ApJ, 684, 558

Rachkovsky D. N., 1962a, Izvestiya Ordena Trudovogo Krasnogo Znameni Krymskoj Astrofizicheskoj Observatorii, 27, 148

Rachkovsky D. N., 1962b, Izvestiya Ordena Trudovogo Krasnogo Znameni Krymskoj Astrofizicheskoj Observatorii, 28, 259

Romero A. D., Córsico A. H., Althaus L. G., Kepler S. O., Castanheira B. G., Miller Bertolami M. M., 2011, ArXiv e-prints

Salpeter E. E., 1955, ApJ, 121, 161

Saviane I., 2011, Very Large Telescope, Paranal Science Operations, FORS User Manual, 89

Schmidt G. D., Bergeron P., Fegley B., 1995, ApJ, 443, 274

Schmidt G. D. et al., 2003, ApJ, 595, 1101

Schmidt G. D., Liebert J., Harris H. C., Dahn C. C., Leggett S. K., 1999, ApJ, 512, 916

Schmidt G. D., Norsworthy J. E., 1991, ApJ, 366, 270

Schoenberner D., 1983, ApJ, 272, 708

Shurcliff W., 1962, Polarized Light: Production and Use. Harvard University Press

Sion E. M., Greenstein J. L., Landstreet J. D., Liebert J., Shipman H. L., Wegner G. A., 1983, ApJ, 269, 253

Stenflo J. O., 1994, Solar magnetic fields : polarized radiation diagnostics / by Jan Olof Stenflo. Dordrecht ; Boston : Kluwer Academic Publishers

Tinbergen J., 1996, Astronomical Polarimetry

Tody D., 1993, in Astronomical Society of the Pacific Conference Series, Vol. 52, Astronomical Data Analysis Software and Systems II, Hanisch R. J., Brissenden R. J. V., Barnes J., eds., p. 173

Tremblay P.-E., Bergeron P., Gianninas A., 2011, ApJ, 730, 128

Unno W., 1956, PASJ, 8, 108

Valyavin G. et al., 2011, ApJ, 734, 17

Vornanen T., Berdyugina S. V., Berdyugin A. V., Piirola V., 2010, ApJ, 720, L52

Wickramasinghe D. T., Ferrario L., 2000, PASP, 112, 873

My Contributions to the Papers

GJ 841B—The second DQ white dwarf with polarized CH molecular bands
I planned and executed the observations. I reduced the data and did the modelling. Main author of the article.

Photometry of two DQ white dwarfs. Search for spots
I planned and executed half of the observations. I reduced the data and developed software for modelling. Main author of the article.

Third article
I planned and executed the observations apart form GJ893.1 which was observed by Andrei Berdyugin. I reduced the data and ran models as well as developed software for modelling. Main author of the article.